

THE RR LYRAE VARIABLES AND HORIZONTAL BRANCH OF NGC 6656 (M22)

ANDREA KUNDER¹, PETER B. STETSON², SANTI CASSISI³, ANDREW LAYDEN⁴, GIUSEPPE BONO^{5,6}, MÁRCIO CATELAN^{7,8}, ALISTAIR R. WALKER¹, LEONARDO PAREDES ALVAREZ¹, JAMES L. CLEM⁹, NORIYUKI MATSUNAGA¹⁰, MAURIZIO SALARIS¹¹, JAE-WOO LEE¹², BRIAN CHABOYER¹³

E-mail: akunder@ctio.noao.edu

AJ accepted

ABSTRACT

The first calibrated broadband *UBVI* time-series photometry is presented for the RR Lyrae variable stars in NGC 6656 (M22), with observations spanning a range of twenty-two years. We have also redetermined the variability types and periods for the RR Lyrae stars identified previously by photographic observations, revising the number of fundamental-mode RR Lyrae variables (RR0) to 10 and the number of first-overtone variables (RR1) to 16. The mean periods of the RR0 and RR1 variables are $\langle P \rangle_{RR0} = 0.66 \pm 0.02$ d and $\langle P \rangle_{RR1} = 0.33 \pm 0.01$ d, respectively, supporting an Oosterhoff II classification for the cluster. The number ratio of RR1- to all RR-type variables is $N_1/N_{RR} = 0.61$, also consistent with an Oosterhoff II designation. Both the RR Lyrae stars' minimum light colors and the blue edge of the RR Lyrae instability strip suggest $E(B-V) = 0.36 \pm 0.02$ mag toward M22. Regarding the HB morphology of M22, we find $(B-R)/(B+V+R) = +0.97 \pm 0.1$ and at least one "gap" located in an unusual part of the blue HB, in the middle of the so-called hot HB stars.

Subject headings: surveys — stars: abundances, distances, Population II — Galaxy: center

1. INTRODUCTION

NGC 6556 (M22) is a relatively massive galactic globular cluster (GC) with $M_V = -8.50$, lying inside the solar circle with $(l, b) = (9.89, -7.55)$ and in relatively close proximity to the Sun, $R_\odot = 3.2$ kpc. These and other basic parameters are listed in (Harris 1996, 2010 edition). Of note is that as far as massive GCs are concerned, M22 is not as heavily crowded as some, with a core radius of

$r_c = 1.33$ arcmin, a central luminosity density of $\rho_0 = 3.63 L_\odot \text{pc}^{-3}$ (2010 edition of Harris 1996) and a tidal radius of $r_t = 27$ pc (Mackey & van den Bergh 2005). Thus despite quite high reddening in which there is likely to be some variation, $E(B-V) = 0.34$ mag, M22 is amenable to ground-based observations.

M22 was first recognized as peculiar when it was discovered that its color-magnitude diagram (CMD) is anomalous: it has a red giant branch (RGB) with a shallower slope than would otherwise be expected based on other metallicity indicators (Butler 1973; Hesser 1976; Hesser et al. 1977; Hesser & Hartwick 1979). Also, importantly, Hesser et al. (1977) found that M22 had a large color spread in the RGB, and therefore linked M22 to the prototypical peculiar GC, ω Cen. Since then, detailed spectroscopic investigations have shown that, like ω Cen, M22 shows variations in its bulk heavy-element content, including iron and elements associated with slow neutron-capture processes (*s*-elements) (e.g., Norris & Freeman 1983; Da Costa et al. 2009; Marino et al. 2009, 2012a).

In particular, from high resolution spectra ($R \sim 38\,000$ to $R \sim 60\,000$) of 35 bright giant stars, Marino et al. (2011a) have shown that the stars in M22 exhibit a large range in their abundance of *s*-elements, in particular the [La/Eu] ratio cleanly divides the sample into two different sub-populations: an *s*-rich stellar component and an *s*-poor one. This was then later also seen in 101 SGB stars using medium-resolution ($R \sim 6400$) spectra (Marino et al. 2012a). There is additionally a strong correlation between [Fe/H] and *s*-element abundance; the *s*-rich stars have a systematically higher [Fe/H] with $\langle [\text{Fe}/\text{H}] \rangle_{s\text{-rich}} = -1.68 \pm 0.02$, whereas the *s*-poor stars are found to have $\langle [\text{Fe}/\text{H}] \rangle_{s\text{-poor}} = -1.82 \pm 0.02$ (Marino et al. 2009). This is a $\Delta[\text{Fe}/\text{H}]$ of 0.14 ± 0.03 dex. The CNO-sum distribution was also found to differ between the *s*-rich and *s*-poor stellar components, on

Based in part on observations made with the European Southern Observatory (ESO) telescopes and obtained from the ESO/ST-ECF Science Archive facility.

This research draws upon data distributed by the NOAO Science Archive. NOAO is operated by the Association of Universities for Research in Astronomy (AURA) under cooperative agreement with the National Science Foundation.

¹ Cerro Tololo Inter-American Observatory, Casilla 603, La Serena, Chile

² Dominion Astrophysical Observatory, NRC-Herzberg, National Research Council, Victoria BC, Canada V9E 2E7

³ INAF-Osservatorio Astronomico di Collurania, Via M. Maggini, I-64100 Teramo, Italy

⁴ Bowling Green State University, Bowling Green, OH 43403, USA

⁵ Dipartimento di Fisica, Università di Roma Tor Vergata, Rome, Italy

⁶ INAF-Osservatorio Astronomico di Roma, via Frascati 33 00040 Monte Porzio Catone, Italy

⁷ Pontificia Universidad Católica de Chile, Departamento de Astronomía y Astrofísica, Av. Vicuña Mackenna 4860, 782-0436 Macul, Santiago, Chile; e-mail: mcatelan@astro.puc.cl

⁸ The Milky Way Millennium Nucleus, Av. Vicuña Mackenna 4860, 782-0436 Macul, Santiago, Chile

⁹ Department of Physics and Astronomy, Louisiana State University, Baton Rouge, LA 70803-4001

¹⁰ Department of Astronomy, School of Science, The University of Tokyo, Japan

¹¹ Astrophysics Research Institute, Liverpool John Moores University, Twelve Quays House, Egerton Wharf, Birkenhead CH41 1LD, UK

¹² Korea Astronomy and Space Science Institute, Daejeon 305-348, Republic of Korea

¹³ Department of Physics and Astronomy, Dartmouth College, Hanover, NH 03755, USA

the order of $\Delta[\text{C} + \text{N} + \text{O}/\text{Fe}] \sim 0.13$ dex, with the *s*-rich one being the CNO-enhanced component (Marino et al. 2009, 2011a). Therefore, M22 is one of the few GCs showing clear evidence of a bimodality in the CNO-sum distribution (as is also seen in ω Cen, e.g., Marino et al. 2012b).

GCs are generally chemically homogeneous when it comes to the abundances of the iron-peak elements (Kraft & Ivans 2003). The well-established counterexamples, such as ω Centauri (Freeman & Rodgers 1975; Norris & Da Costa 1995; Pancino et al. 2002), M54 in the Sagittarius dSph (Bellazzini et al. 2008; Carretta et al. 2010a; Saviane et al. 2012), NGC 2419 (Cohen 2010; Mucciarelli et al. 2012), NGC 1851 (Carretta et al. 2010b), M22 (Da Costa et al. 2009; Marino et al. 2009) and Terzan 5 (Ferraro et al. 2009) may have a different origin than the other GCs. For example, they could have an extragalactic origin, such as being the remnant of a dwarf galaxy tidally disrupted by the MW. That these GCs have a peculiar origin is also suggested because they are some of the most massive GCs in the Galaxy and have different kinematics (e.g., retrograde rotation) than many “normal” GCs (Lee et al. 2007).

Photometrically, the two distinct sub-populations present in M22 have been traced along the RGB using Strömgren filters (Milone et al. 2012a), and along the SGB using optical *Hubble Space Telescope* (*HST*) filters (Piotto et al. 2012). The interpretative analysis provided by Cassisi et al. (2008) and Sbordone et al. (2011) suggests that the observed split along these evolutionary sequences can be understood as due to the bimodality in the CNO-sum and the observed light-element anticorrelations, respectively, the latter now understood to be a ubiquitous feature of GCs (Carretta et al. 2009a,b).

The spectroscopic study of multiple populations in Galactic GCs has recently been extended to the HB, e.g., M4, Marino et al. (2011b); NGC 1851, Gratton et al. (2012); NGC 2808, Gratton et al. (2011) and 47 Tuc, Milone et al. (2012b), Gratton et al. (2013). On the basis of these measurements a scenario is emerging in which Na-poor/O-rich stars, the first generation progeny, are located in the red portion of the HB, whereas Na-rich/O-poor stars, the stars belonging to the second generation, are distributed along the blue portion of the HB. Since the presence of a Na-O anticorrelation has to be accompanied by (at least a moderate) helium enhancement, and He-rich stars are expected on theoretical grounds to populate the bluest portion of the HB distribution, these empirical findings provide plain evidence that the HB morphology is greatly affected by the multiple-population phenomenon. In the case of NGC 1851, spectroscopy supplemented with an accurate analysis of both the HB morphology and the pulsation properties of RR Lyrae stars (Kunder et al. 2013a) has been used to shed more light on the detailed distribution of the various sub-populations along the HB of this peculiar GC. Very recently, the first spectroscopic tracing of sub-populations along the HB of M22 has been carried out by Marino, Milone & Lind (2013), finding that all the (seven) red HB stars (including 3 RR Lyrae variables) analyzed are barium-poor and sodium-poor and belong to the first generation of stars.

In this paper we present new *UBVI* photometry of

M22, based on original and archival observations, which has allowed a more detailed study of the RR Lyrae instability strip than has previously been possible, including the discovery of additional RR Lyrae stars and the first calibrated light curves of the complete M22 RR Lyrae variable sample. We will use these data to seek evidence of the metallicity and generational dichotomies described above among the RRL in M22.

2. OBSERVATIONS

The observations come from co-author Peter B. Stetson’s (PBS) data archive and the details are given in Table 1. The last column in the table with the heading “Multiplex” refers to the number of individual CCDs in the camera used for the observing run. Standard DAOPHOT/ALLFRAME procedures (Stetson 1987, 1990, 1994) were used to perform profile-fitting photometry with aperture growth-curve corrections. The calibration of the instrumental data is to the Johnson/Kron-Cousins *UBVI* photometric system defined by (Landolt 1992), and was carried out as described by Stetson (2000, 2005). The observations are contained within 61 datasets, where a dataset is either the complete body of data from one CCD on one photometric night or the body of data from one CCD on one or more non-photometric nights during the same observing run. Therefore the number of datasets and the number of images will be different, as datasets, individually calibrated to the Landolt system, may be broken up to compensate for e.g., changing weather conditions. Of the 61 datasets, 35 are considered photometric, and the remaining 26 are considered non-photometric. The 35 photometric datasets are used to set up local standards in the field of M22, using nightly calibration equations that include linear and quadratic color terms as well as linear extinction terms; a color-extinction term is also employed for the *B* filter. These local standards are then used to determine the photometric zero points of individual CCD images obtained on non-photometric nights.

The maximum number of calibrated magnitude measurements for any one star is 24 in *U*, 154 in *B*, 206 in *V*, and 44 in *I*. There was one photometric night in which *R*-band data was obtained, but we consider that insufficient for a reliable photometric calibration, and a discussion of M22 *R*-band photometry is not presented here. However, the *R*-band images were included in the ALLFRAME reductions to aid in the completeness and astrometric precision of the catalog. Our final catalog includes 620,730 objects with photometric measurements and spans a field roughly 38.5 arcminutes east-west by 49.2 arcminutes north-south. There are 525,585 objects with “useful” measurements (arbitrarily defined as $\sigma(\text{magnitude}) < 0.10$ mag) in *B*, *V*, and *I*; 55,910 of these also have useful (same definition) photometry in *U*. There are a further 96,857 objects with astrometric information only (46.8 by 49.2 arcminutes).

The astrometry is carried out as in Kunder et al. (2013b), tied to the U.S. Naval Observatory (USNO) A2.0 Astrometric Reference Catalog. Therefore we believe our positions are on the USNO-A2.0 system with an accuracy well within $0''.1$, and are internally precise to better than $0''.03$.

TABLE 1
M22 OBSERVATIONS

| Run ID | Dates | Telescope/Camera/Detector | <i>U</i> | <i>B</i> | <i>V</i> | <i>R</i> | <i>I</i> | Multiplex |
|--------------|----------------|-----------------------------|----------|----------|----------|----------|----------|-----------|
| 1 bond21 | 1991 Sep 23 | CTIO 0.9m 772 | – | 2 | 2 | – | – | |
| 2 emmi5 | 1993 Jul 17–18 | ESO NTT 3.6m EMMI | – | 20 | 21 | – | – | |
| 3 apr97 | 1997 Apr 16 | ESO Dutch 0.9m Tektronix 33 | – | – | 8 | – | 8 | |
| 4 bond6 | 1998 Apr 22 | CTIO 0.8m Tek2K_3 | 1 | 1 | 1 | – | 1 | |
| 5 dmd | 1998 Jun 25 | JKT 1.0m TEK4 | – | – | 2 | – | 3 | |
| 6 wfi9 | 1999 May 15 | ESO/MPI 2.2m WFI | – | 4 | 3 | – | 3 | ×8 |
| 7 wfi12 | 1999 Jul 12 | ESO/MPI 2.2m WFI | – | 1 | 4 | – | 2 | ×8 |
| 8 wfi10 | 2000 Jul 07 | ESO/MPI 2.2m WFI | – | 4 | 4 | – | 3 | ×8 |
| 9 ct36aug00 | 2000 Aug 30–31 | CTIO 0.9m Tek2K_3 | – | 78 | 78 | – | – | |
| 10 wfi5 | 2002 Jun 18 | ESO/MPI 2.2m WFI | – | 6 | 6 | – | 6 | ×8 |
| 11 susi03may | 2003 May 31 | ESO NTT 3.6m SUSI | 8 | – | 8 | – | – | ×2 |
| 12 wfi26 | 2004 Jun 26 | ESO/MPI 2.2m WFI | – | 4 | 6 | – | – | ×8 |
| 13 fors20605 | 2006 May 29 | ESO VLT 8.0m FORS2 | – | – | 3 | 5 | 3 | ×2 |
| 14 fors0707 | 2007 Jul 03–05 | ESO VLT 8.0m FORS1 | 1 | – | 38 | – | – | ×2 |
| 15 efosc09 | 2009 Apr 20–29 | ESO NTT 3.6m EFOSC LORAL | 16 | 69 | 10 | 3 | – | |
| 16 ct12aug | 2012 Aug 19–21 | CTIO 0.9m Tek2K_3 | 20 | 15 | 45 | – | 15 | |

Notes:

1 Observer H. E. Bond 2 Observers “SAV/ZAGGIA” 3 Observer A. Rosenberg? 4 Observer H. E. Bond 5 Observer “DMD” 6 Program identification 163.O-0741(C) 7 Program identification unknown, observer unknown 8 Program identification 065.L-0463, observer Ferraro 9 Observers A. Walker & D. Walker 10 Program identification 69.D-0582(A) 11 Program identification 71.D-0175(A) 12 Program identification 073.D-0188(A) 13 Program identification 077.D-0775(A) 14 Program identification 079.D-0893(A) 15 Program identification 083.D-0544(A) 16 Proposal ID 2012B-0178, observers A. Kunder, L. Paredes Alvarez

TABLE 2
RR LYRAE STARS IN M22

| Name | R.A. (J2000.0) | Decl. (J2000.0) | Period (d) | $\langle U \rangle$ | $\langle B \rangle$ | $\langle V \rangle$ | $\langle I \rangle$ | A_U | A_B | A_V | A_I | Type | R_{proj} ($'$) | Separation Index | Comment |
|-------|-------------------|--------------------|------------|---------------------|---------------------|---------------------|---------------------|-------|-------|-------|-------|--------------|-----------------------|---------------------|-------------------------|
| V1 | 18 36 19.55 | -23 54 32.7 | 0.615541 | 15.15 | 15.00 | 14.27 | 13.26 | 1.35 | 1.48 | 1.15 | 0.69 | RR0 | 1.1 | 5.9 | period in- creasing? |
| V2 | 18 36 34.90 | -23 53 06.3 | 0.641718 | 14.81 | 14.79 | 14.10 | 13.19 | 1.16 | 1.21 | 0.93 | 0.57 | RR0 | 3.0 | 5.5 | |
| V3 | 18 36 37.99 | -23 47 14.9 | 0.539559: | - | 16.49 | 15.64 | 14.69 | - | - | - | - | RR0 | 7.1 | | ^a |
| V4 | 18 36 23.35 | -23 55 29.1 | 0.716393 | 15.09 | 14.94 | 14.17 | 13.15 | 1.02 | 0.98 | 0.80 | 0.52 | RR0 | 1.2 | 4.8 | |
| V6 | 18 36 18.24 | -23 56 03.4 | 0.638486 | 14.91 | 14.80 | 14.10 | 13.14 | 1.35 | 1.37 | 1.10 | 0.70 | RR0 | 2.3 | 6.3 | ^b |
| V7 | 18 35 57.60 | -23 47 40.5 | 0.649523 | 14.94 | 14.81 | 14.10 | 13.20 | 1.19 | 1.44 | 1.26 | 0.70 | RR0 | 9.3 | 10.7 | |
| V10 | 18 36 20.92 | -23 56 27.1 | 0.646028 | 14.93 | 14.82 | 14.13 | 13.16 | 1.05 | 1.41 | 1.15 | 0.64 | RR0 | 2.3 | 6.1 | |
| V12 | 18 36 23.75 | -23 55 38.8 | 0.322622 | 15.00 | 14.78 | 14.19 | 13.38 | 0.61 | 0.57 | 0.44 | 0.27 | RR1 | 1.4 | 5.6 | |
| V13 | 18 36 28.64 | -23 51 39.5 | 0.672530 | 14.87 | 14.74 | 14.06 | 13.14 | 1.10 | 1.36 | 1.08 | 0.65 | RR0 | 2.9 | 6.5 | |
| V15 | 18 36 32.07 | -23 55 40.6 | 0.370922 | 14.98 | 14.84 | 14.21 | 13.34 | 0.49 | 0.56 | 0.41 | 0.23 | RR1 | 2.5 | 6.2 | |
| V16 | 18 36 36.97 | -23 54 33.2 | 0.325293 | 15.06 | 14.80 | 14.24 | 13.44 | 0.49 | 0.54 | 0.44 | 0.24 | RR1 | 3.3 | 5.6 | |
| V18 | 18 36 16.14 | -23 47 14.9 | 0.321059 | - | 14.65 | 14.11 | 13.35 | - | 0.57 | 0.46 | 0.30: | RR1 | 7.3 | 10.3 | |
| V19 | 18 36 20.58 | -23 52 17.2 | 0.383621 | 15.06 | 14.75 | 14.19 | 13.33 | 0.55 | 0.58 | 0.46 | 0.35 | RR1 | 2.2 | 7.0 | |
| V20 | 18 36 14.79 | -23 56 32.9 | 0.756134 | 14.98 | 14.84 | 14.10 | 13.09 | 0.80 | 0.93 | 0.70 | 0.43 | RR0 | 3.2 | 6.1 | |
| V21 | 18 36 25.74 | -23 52 57.9 | 0.327134 | 14.73 | 14.64 | 14.07 | 13.30 | 0.42 | 0.54 | 0.40 | 0.23 | RR1 | 1.4 | 5.2 | |
| V22* | 18 35 03.8 | -23 50 58.2 | 0.6245374 | - | - | 13.17 | - | - | - | 0.41 | - | field RR0 | 20.3 | | V3853 Sgr |
| V23 | 18 36 23.01 | -23 54 41.4 | 0.581019: | 15.36 | 14.93 | 14.28 | 13.32 | 1.25 | 1.37 | 1.02 | 0.62 | RR0 | 0.5 | 5.2 | |
| V24 | 18 36 24.04 | -23 54 29.4 | - | 14.1 | 13.1 | 11.3 | 9.3 | - | - | - | - | NV | 0.4 | | not a vari- able |
| V25 | 18 36 46.29 | -23 48 02.2 | 0.399985 | 15.02 | 14.83 | 14.18 | 13.30 | 0.47 | 0.62 | 0.46 | 0.31 | RR1 | 8.4 | 9.5 | Blazhko? V2592 Sgr |
| V27* | 18 35 28.92 | -23 45 25.3 | 0.34278 | - | - | 13.33 | - | - | - | 0.32 | - | field RR1 | 16.4 | | |
| V29 | 18 36 30.85 | -23 41 03.2 | 0.471584 | - | 14.79 | 14.21 | 13.37 | - | 0.45 | 0.36 | - | field RR1 | 13.3 | | NSV 11080 |
| KT-12 | 18 36 30.93 | -23 53 48.8 | 0.443610 | - | 17.28 | 16.56 | 15.59 | - | 1.18 | 0.93 | 0.50 | RR0 | 1.8 | | bulge star |
| KT-14 | 18 36 30.67 | -23 53 53.8 | 0.371984 | 14.85 | 14.69 | 14.07 | 13.25 | 0.39 | 0.35 | 0.30 | 0.18 | RR1 | 1.7 | 4.3 | Blazhko? blending? |
| KT-16 | 18 36 30.36 | -23 57 12.9 | 0.2819 | 14.95 | 14.71 | 14.17 | 13.45 | 0.07 | 0.11 | 0.07 | 0.05 | RR1 | 3.3 | 6.6 | |
| KT-26 | 18 36 23.15 | -23 53 23.3 | 0.370960 | 15.00 | 14.74 | 14.12 | 13.29 | 0.17 | 0.32 | 0.17 | 0.14 | RR1 | 0.9 | 2.1 | |
| KT-36 | 18 36 15.88 | -23 56 06.9 | 0.315182 | 14.99 | 14.75 | 14.17 | 13.41 | 0.36 | 0.46 | 0.37 | 0.22 | RR1 | 2.7 | 7.2 | |
| KT-37 | 18 36 13.17 | -23 53 46.8 | 0.296058 | 14.94 | 14.72 | 14.16 | 13.42 | 0.14 | 0.17 | 0.13 | 0.07 | RR1 | 2.7 | 6.2 | |
| KT-55 | 18 36 23.23 | -23 53 57.9 | 0.658735 | 15.07 | 14.85 | 14.14 | 13.17 | 0.86 | 1.3 | 0.75 | 0.4: | RR0 | 0.4 | 4.1 | Blazhko? |
| NV1 | 18 35 59.11 | -23 57 13.1 | 0.305811 | 14.92 | 14.66 | 14.14 | 13.41 | 0.24 | 0.28 | 0.22 | 0.11 | RR1 | 6.9 | 8.7 | |
| NV2 | 18 36 02.96 | -23 50 29.4 | 0.332917: | 99.99 | 14.83 | 14.23 | 13.45 | 9.99 | 0.25 | 0.16 | 0.15: | RR1 | 6.5 | 3.1 | period un- certain |
| NV3 | 18 36 29.52 | -24 01 32.6 | 0.334020 | 99.99 | 14.58 | 14.05 | 13.38 | 9.99 | 0.48 | 0.40 | - | RR1 | 7.4 | 5.4 | |
| NV4 | 18 36 31.67 | -23 49 30.3 | 0.287082 | 15.08 | 14.72 | 14.18 | 13.42 | 0.35 | 0.16 | 0.11 | 0.08 | RR1 | 5.2 | 8.5 | |

* insufficient observations (star is outside field of view), data presented here are taken from the ASAS survey Pojmański (2000)

^a inadequate phase coverage, too faint to be cluster RRL

^b some light curve instability seen, e.g., phase jumps

3. RESULTS

3.1. RR Lyrae variables

The first variable stars (V1-16) in M22 were discovered more than a century ago by Bailey (1902). Gradually additional variables were discovered: V17 in Shapley (1927), V18-25 by Sawyer (1944) and V26-31 by Hoffleit (1972). Wehlau & Sawyer Hogg (1977) published the discovery of V32 and V33, Lloyd Evans (1978) published the discovery of V34 and V35, and Kravtsov et al. (1994) identified V36-43, although the membership of these variables is uncertain. Finally the first results from CCD observations were presented by Kaluzny & Thompson (2001) resulting in 36 new variables. They were not able to determine periods for the seven RR Lyrae variables they detected, and provide approximate B and V calibration of their photometry. Pietrukowicz & Kaluzny (2003) identified eight more variables and both Anderson et al. (2003) and Pietrukowicz et al. (2005) announced one new variable. This brings the number of M22 variables to ninety, of which twenty-seven are RR Lyrae variables.

The sample of RR Lyrae stars in and around M22 is presented in Table 2. We estimate that the astrometry presented is accurate to better than 0.1 arcseconds and the photometry is accurate to ~ 0.01 mag. The columns contain (1) the name of the variable as given in the 2011 update of M22 in the Clement et al. (2001) catalog, (2) the right ascension in hours, minutes and seconds (epoch J2000), (3) the declination in degrees, arcminutes and arcseconds, (4) the period in days, (5-8) the magnitude-weighted mean U , B , V , and I , respectively, (9-12) the U -, B -, V - and I -amplitude, respectively, (13) the type of variable, (14) the projected radius (in arcmin) from the star to cluster center (R_{proj}), (15) the separation index (as defined in Stetson, Bruntt & Grundahl 2003) and (16) any comments.

The light curves of the RR0 Lyrae variables are presented in Figure 1, and the RR1 stars are shown in Figure 2. The template-fitting routines from Layden (1998) and Layden & Sarajedini (2000) were used to fit the data, but a Fourier decomposition was used for their mean magnitude and amplitude parameters. Our observations do not cover the RR Lyrae variables V22 and V27, as they lie 16.5 and 20 arcminutes, respectively, from the cluster center. These stars were observed as part of the ASAS survey, and their bright mean magnitudes (~ 1 mag brighter) suggest that both these stars are too bright to belong to the cluster. Further evidence that these two stars belong to the field population comes from their amplitudes, which are small for their pulsation periods (see Table 2), suggesting they are more metal-rich than the rest of the M22 RR Lyrae stars. Our observations also provide insufficient phase coverage for V3, but our photometry clearly suggests that this star is too faint to belong to the cluster. It has a magnitude similar to the majority of the RR Lyrae variables located in the Galactic bulge (Kunder et al. 2008; Pietrukowicz et al. 2012). Similarly the RR Lyrae variable KT-12 is too faint to belong to M22, and also likely belongs to the bulge population; our phase coverage for this star allows robust $UBVI$ magnitudes to be determined, which are presented in Table 2.

We have discovered four new low amplitude RR Lyrae

stars, presented in Figure 3. These stars are all located ~ 6 arcminutes from the center of the cluster; there are only 3 other M22 RR Lyrae variables at comparably large distances, the other M22 RR Lyrae variables lying at a mean distance of 2 arcminutes from the center. The specific frequency of RR Lyrae stars in M22 is $S_{RR}=10.4$ where $S_{RR} = N_{RR} \times 10^{0.4(7.5+M_V)}$, and $M_V=-8.50$ (Harris 1996, 2010 update) is the cluster’s integrated absolute magnitude in V .

The mean periods for the 10 RR0 Lyrae stars and 16 RR1 stars are $\langle P \rangle_{RR0} = 0.66 \pm 0.02$ d and $\langle P \rangle_{RR1} = 0.33 \pm 0.01$ d, respectively. The ratio of RR1 to total RR Lyrae stars, N_1/N_{RR} , is 0.61. As Figure 4 shows, the mean periods of the RR0 Lyrae stars are similar to those found in the typical Oosterhoff II (OoII) clusters, as is the large N_1/N_{RR} ratio Catelan (e.g., 2009).

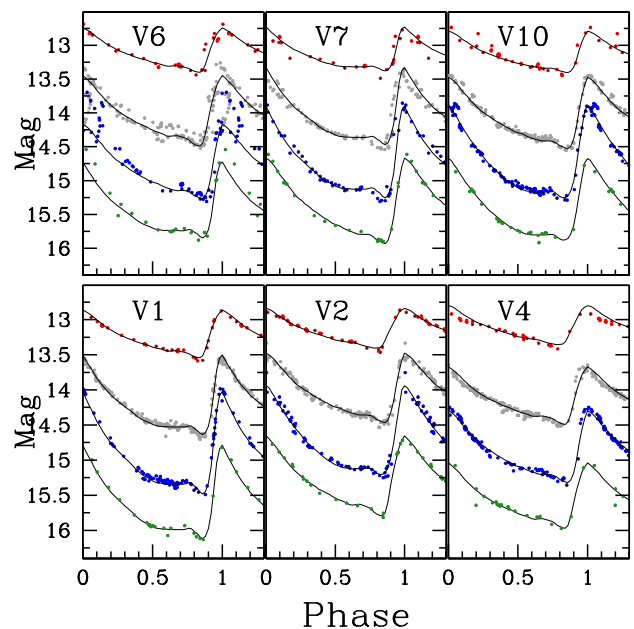


FIG. 1.— Presentation of the phased $UBVI$ light curves of the fundamental mode RR Lyrae variables in M22.

A significant fraction of RR Lyrae variables exhibit the Blazhko effect (hereafter also referred to as “Blazhkocity”), which can be described as long-term, sometimes periodic but often irregular amplitude and/or phase modulations (e.g., Blazhko 1907; Klepikova 1956; Benkő et al. 2010; Buchler & Kolláth 2011; Le Borgne et al. 2012). This effect is not understood theoretically. The only systematic survey carried out to determine the frequency of light curve modulation of RR0 Lyrae stars is the Konkoly Blazhko Survey (KBS, Jurcsik et al. 2009). KBS1 consists of 30 field RR0 Lyrae stars with $P_{RR0} < 0.50$ d, and it was found that $\sim 47\%$ exhibit Blazhkocity (Jurcsik et al. 2009). Similarly, from 124 field RR0 stars with periods ranging from 0.55–0.60 d, KBS2 reports a $\sim 43\%$ incidence of stars with Blazhkocity (Sódor et al. 2012). The case for the RR1 stars is more unclear. Blazhkocity is usually not seen in RR1 variables (it is thought that the Blazhko effect occurs in $\sim 5\%$ of RR1 variables; Moskalik & Poretti 2003; Kolenberg 2011) although recent studies of the

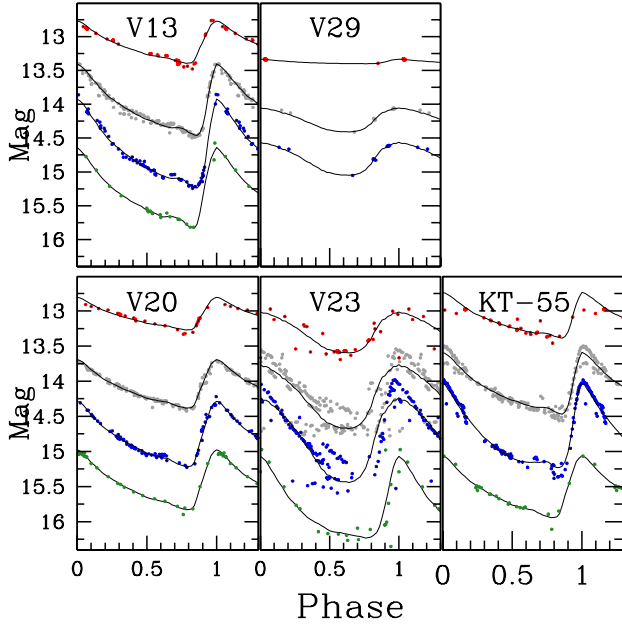


FIG. 1.— RR0 Lyrae light curves continued

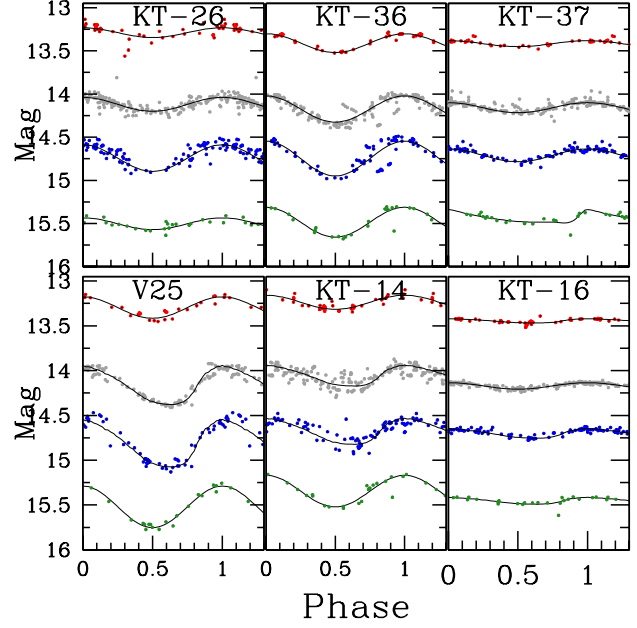
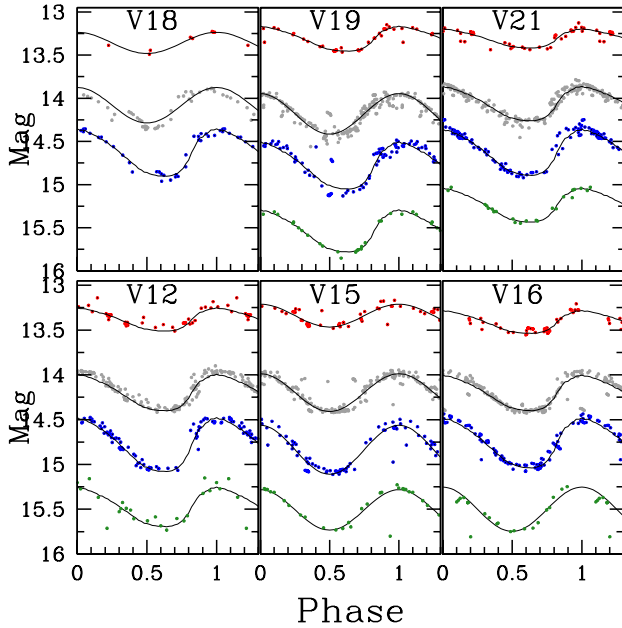
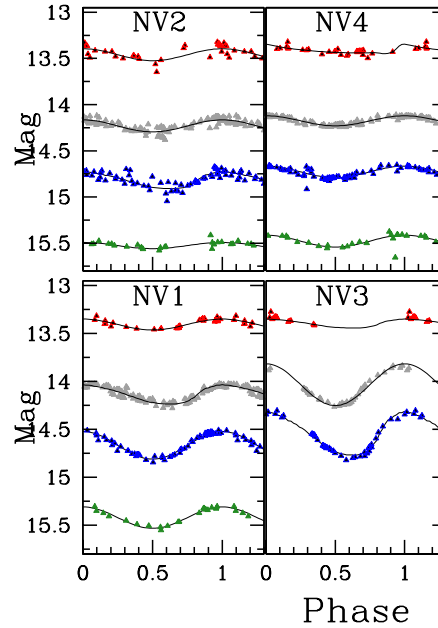


FIG. 2.— RR1 light curves continued

FIG. 3.— Presentation of the phased *UBVI* light curves of the first overtone RR Lyrae variables in M22.FIG. 4.— Presentation of the phased *UBVI* light curves of the newly discovered RR Lyrae variables in M22.

GCs NGC 2808 and M53 have revealed RR Lyrae populations with large ($> 50\%$) RR1 Blazhko percentages (Arellano Ferro et al. 2012; Kunder et al. 2013b).

The RR0 stars in M22 with light curve modulation include V6, V23 and KT-55 (see Figure 1). However, upon closer examination, the scatter in the light curve of V6 appears to be caused by various phase jumps, with no obvious cyclic variation of the pulsation amplitude such as seen in stars exhibiting Blazhko. V23 also has a light curve more indicative of a star with a rapidly changing or erratic period, as opposed to a star with Blazhko. KT-55, on the other hand, may be exhibit-

ing Blazhko, particularly as amplitude modulation at maximum light is seen in the *V* light curve (where there are more observations.) Assuming that only KT-55 exhibits Blazhko, this suggests a relatively small ($\sim 10\%$) incidence of Blazhko RR0s in M22.

However, although our observations span many years, the most useful set of observations were taken over three nights in 2012 and such irregular spacing is not sufficient to derive either Blazhko periods or secondary periodicities with any confidence. Without Blazhko periods, it is difficult to know for certain whether the scatter in the light curves is indeed due to the Blazhko effect or

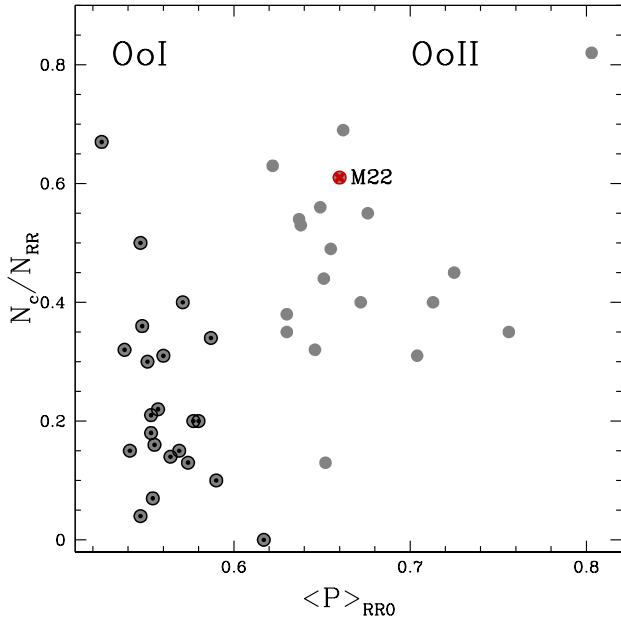


FIG. 4.— The ratio of RR1 to total RR Lyrae stars, N_1/N_{RR} , shown as a function of average RR0 period, based on the compilation presented in Catelan 2009. The properties of M22 derived here indicated this cluster is an OoII-type GC.

whether the light curve scatter is due to other phenomena such as unstable periods, large period-change rates (e.g., Le Borgne et al. 2007; Kunder et al. 2011), secondary periods (e.g., Fitch & Szeidl 1976; Peniche et al. 1989; Moskalik & Poretti 2003), period doubling (e.g., Szabo et al. 2010), and/or photometric anomalies such as blending compounded by variable seeing conditions. We have searched the stars for secondary periods, and find no firm evidence of secondary periods in the sample. However, it is worth noting that double-mode RR Lyrae stars usually reside in metal-poor OoII-type clusters (e.g., Clement & Walker 1991) so the environment of M22 could be receptive to such pulsators.

We have also searched for trends between light curve scatter and stellar brightness to see whether any faint neighboring stars were contaminating the stellar PSF profile (as blending would make the RRL brighter, while blending combined with variable seeing could increase the light curve scatter). No systematic trend in perceived stellar brightness as a function of radial distance is seen, and no trends in stellar brightness as a function of Blazhkoicity are found either. However, it is worth mentioning that many of the stars with light curve scatter are located closer to the center of the cluster. We have also searched for trends in a stars' separation index, where the separation index is defined by Stetson, Bruntt & Grundahl (2003). The larger the separation index, the less a given star is contaminated by its known neighbors. All of the RR Lyrae variables have separation indices greater than zero, although there are two stars (one exhibiting light curve scatter and one that does not) with a separation index less than or equal to three. A separation index of 3.0 indicates that the light of a star is contaminated by its *known* neighbors at a 6% level; since the known neighbors are accounted for in the PSF fits, the residual contamination by these stars should be at least an order

of magnitude less. In summary, we stress that we have no specific evidence that the light curve scatter seen is caused by blending. But we do remain alert to the fact that PSF fitting in crowded fields observed under different seeing conditions is challenging. It is also possible that incorrect cycle counts spanning long intervals without observations can lead to inaccurate periods, but we stress that the periods we have derived are statistically superior to alternative periods requiring different numbers of cycles over the time span that we have covered.

3.2. RR Lyrae Distance

The mean apparent magnitude for the RR Lyrae variables is $\langle m_{V,RR} \rangle = 14.15 \pm 0.02$ mag, where the confidence interval is the standard error of the mean. This is in excellent agreement with the Harris (1996) value of $m_{V,HB} = 14.15$, which lists the mean V magnitude of the horizontal branch, V_{HB} . It also agrees well with the Monaco et al. (2004) estimate of $m_{V,HB} = 14.17 \pm 0.25$ mag, found from averaging the V magnitudes of the RR Lyrae stars observed at random phases.

The absolute magnitudes of the RR0 variables can be estimated using:

$$M_V = 0.23[\text{Fe}/\text{H}]_{\text{CG97}} + 0.931 \quad (1)$$

from Catelan & Cortés (2008), where $[\text{Fe}/\text{H}]_{\text{CG97}}$ is the metallicity in the Carretta & Gratton (1997) scale. Adopting $[\text{Fe}/\text{H}] = -1.75$ dex on the Kraft & Ivans (2003) scale (Marino et al. 2009; Da Costa et al. 2009), $[\text{Fe}/\text{H}]_{\text{CG97}} = -1.55$ dex, and therefore the absolute magnitudes of the RR Lyrae variables in M22 are $M_V = 0.57 \pm 0.13$ mag. Similarly, using a quadratic relation between RR Lyrae absolute magnitude and metallicity from Bono, Caputo, & di Criscienzo (2007):

$$M_V = 0.08[\text{Fe}/\text{H}]^2 + 0.50[\text{Fe}/\text{H}] + 1.19 \quad (2)$$

the RR Lyrae absolute magnitudes are $M_V = 0.56 \pm 0.08$. A brighter $M_V = 0.40 \pm 0.07$ is found when using the Benedict et al. (2011) $M_V - [\text{Fe}/\text{H}]$ relation, however, suggesting that the level of agreement between independent M_V measurements is as large as ~ 0.2 mag.

The level of evolution off the ZAHB can also affect an RR Lyrae star's absolute magnitude in V by ~ 0.08 mag (e.g., Sandage 1990; Clementini et al. 2003), as can an RR Lyrae star's helium content, alpha-element abundance and CNO content. The metallicity bimodality in M22 of $\Delta[\text{Fe}/\text{H}] \sim 0.14$ (see the Introduction), corresponds to variation of 0.04 mag in M_V .

It is worth noting that the Catelan & Cortés (2008) absolute magnitude relationship assumes a helium abundance of $Y = 0.23$, an $[\alpha/\text{Fe}] = +0.31$, and no CNO enhancement. The Bono et al. (2007) relation is based on synthetic HB simulations and a large sample of Galactic globular clusters; therefore it assumes a He, $[\alpha/\text{Fe}]$ and CNO typical of MW GCs. If the He, $[\alpha/\text{Fe}]$ and CNO of the M22 RR Lyrae stars is abnormal, the RR Lyrae absolute magnitudes will be slightly affected.

Using the above determined M_V of $M_V = 0.57 \pm 0.12$, the apparent distance modulus of M22, based upon the RR Lyrae variables, is $(m - M)_{V,RR} = 13.58 \pm 0.13$. Using $E(B - V) = 0.36$ mag (see below, §3.5), we obtain a true distance modulus $(m - M)_{0,RR} = 12.46 \pm 0.13$, which implies a geometric distance of 3.1 ± 0.2

kpc. The Benedict et al. (2011) absolute magnitude of $M_V=0.40\pm 0.07$ results in $(m-M)_{V,\text{RRL}}=13.75\pm 0.11$, and a true distance modulus $(m-M)_{0,\text{RRL}}=12.67\pm 0.12$ or 3.4 ± 0.2 kpc.

RR Lyrae period-luminosity PL relations in IJK are powerful in that they are not as sensitive to evolutionary effects as the bluer passbands, leading to the presence of tighter absolute magnitude relations (e.g., Catelan et al. 2004). The reddening is also not as severe in these passbands. Using the Catelan et al. (2004) relation of

$$M_I = 0.471 - 1.132\log P + 0.205\log Z \quad (3)$$

and $Z=0.0006$ ($[\text{Fe}/\text{H}]=-1.77$, $Y=0.23$, $\alpha/\text{Fe}=+0.35$, no CNO enhancement), and using $E(B-V)=0.36$ mag, a true distance modulus $(m-M)_{0,\text{RRL}}=12.50\pm 0.10$ is found. This translates to a geometric distance of 3.2 ± 0.2 kpc, and is in excellent agreement with the distances determined from the $M_V-[\text{Fe}/\text{H}]$ relations above.

3.3. The RR Lyrae Color-Magnitude Diagram

Figure 5 gives an expanded view of the HB. As suggested earlier and demonstrated in §3.5, there is significant differential reddening across the face of M22 that increases the scatter in Figure 5. The RR0 stars provide a means to quantify and correct for this effect. The arrows in Figure 5 show the originally observed positions (squares) and the positions corrected for differential reddening (arrow heads) based on the mean reddening of $E(V-I) = 0.46$ and the stars' colors in Table 5. Thus, the arrow heads should be compared to the evolutionary model tracks; this indicates that the RR0 in M22 are likely lower mass stars evolved from BHB rather than higher mass stars living on the red end of the ZAHB. The arrows also give a sense for how much the RR1 and non-variable BHB stars in Figure 5 are affected by differential reddening.

As mentioned in the Introduction, the stars in M22 can be roughly divided into two metallicity groups – the s -rich and the s -poor stars (e.g., Marino et al. 2011a; Alves-Brito et al. 2012), with $[\text{Fe}/\text{H}]_{s\text{-rich}} = -1.68 \pm 0.02$ and $[\text{Fe}/\text{H}]_{s\text{-poor}} = -1.82 \pm 0.02$ (Marino et al. 2009). The appropriate theoretical models from the BaSTI archive (Pietrinferni et al. 2004, 2006, 2009) are overplotted in Figure 5 to illustrate how the RR Lyrae stars in M22 are matched by theoretical evolutionary predictions. In particular, the Zero Age Horizontal Branch (ZAHB) loci corresponding to different assumptions about the chemical mixtures are shown: a ZAHB locus for an α -enhanced mixture with $[\text{Fe}/\text{H}] = -1.84$, and a ZAHB locus corresponding to a mixture where the CNO sum is enhanced with respect to the standard α -enhanced mixture and $[\text{Fe}/\text{H}] = -1.58$. For the CNO-enhanced ZAHB locus, the BaSTI models available account for a CNO-sum enhancement of approximately $[\text{C} + \text{N} + \text{O}/\text{Fe}] \approx 0.3$ dex. However, as a smaller CNO-enhancement of ~ 0.13 dex is found from the spectroscopic measurements of M22, a correction to both magnitude and color index of the models is made to account for this difference¹⁴. For the standard

¹⁴ This correction has been estimated by comparing the model predictions for various levels of CNO-enhancement discussed in Pietrinferni et al. (2009).

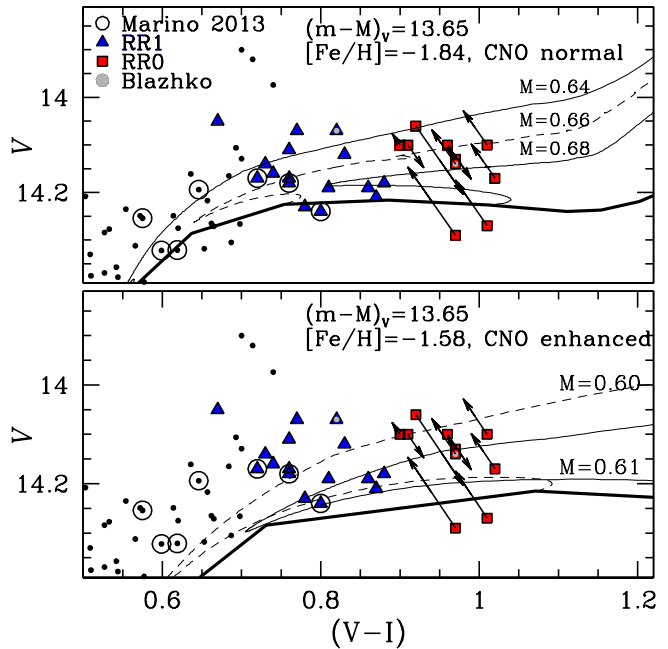


FIG. 5.— The M22 Instability strip in V versus $V-I$. Stars near the M22 instability strip are marked with points as defined in the key. Curves are BaSTI models of the ZAHB (bold) and evolutionary tracks for different masses (M) for a metal-poor, CNO-normal case (top) and a metal-rich, CNO-enhanced case (bottom). Arrows indicate the differential reddening corrections for RR0 stars described in §3.3.

α -enhanced stellar locus, a shift of $+0.05$ mag in V to the BaSTI ZAHB is applied to account for the updated conductive opacities provided by Cassisi et al. (2007). This shift is important to obtain a self-consistent comparison with the CNO-enhanced ZAHB, which has been computed accounting for the updated conductive opacities (see Cassisi et al. 2007, for a detailed analysis of this issue).

We adopt a reddening $E(B-V) = 0.36$ and a distance modulus of $(m-M)_V = 13.65$ mag for the theoretical comparison in Figure 5. This distance modulus is within the range of the distances obtained from the RR Lyrae variables discussed above in §3.2 and was chosen because it allows the lower envelope of the observed HB star distribution for the standard α -enhanced ZAHB to match the BaSTI models.

In each panel of Figure 5, the evolutionary tracks of some selected HB stellar models are also shown. Figure 5 therefore shows the comparison between observational data and theoretical models. Because the theoretical models in both panels are located at approximately the same position in the CMD, it is difficult to trace the origin of the RR Lyrae population – that is, to assess whether they belong to the first generation (the canonical α -enhanced one) or to the second generation (the more metal-rich, CNO-enhanced one). However, it is worth noting that, that if one assumes that the RR stars are (mainly) associated with the first generation, then their location in the CMD is well matched by the evolutionary pattern of HB models during the main core He-burning stage. In particular, BaSTI models also indicate that in such a scenario, most of the M22 RR Lyrae stars have a rather small mass range of $\sim 0.66 - 0.68 M_\odot$. We note

that it has been shown spectroscopically that three (blue) RR1 variables in M22 are metal-poor with a normal CNO content (Marino et al. 2013) and therefore likely belong to the first generation.

On the other hand, if one assumes that the RR Lyrae stars belong to the second generation, the theoretical prediction is that these variables are brighter than the ZAHB, and that their location (at least of the majority of them) could be (mainly) explained as due to stars crossing the instability strip during their off-ZAHB evolution. In this scenario, their predicted masses would be $\sim 0.60 - 0.61 M_{\odot}$.

It is obvious that spectroscopic investigations of the chemical composition of the M22 RR Lyrae stars, and in particular the measurement of O and Na abundances, would help in discriminating between these scenarios. However, due to the large difference in the evolutionary rates between HB stars experiencing their major core He-burning stage and those crossing the RR Lyrae when moving from the blue side of the HB distribution towards the Asymptotic Giant Branch, some useful hint for disentangling the evolutionary origin of these variable stars could be obtained by the analysis of the secular pulsation period changes (however see e.g., Le Borgne et al. 2007; Kunder et al. 2011, for the difficulties in associating period change rates to the evolutionary status of a star).

3.4. Period-Amplitude Diagram

The period-amplitude (PA) diagram for the RR Lyrae stars is shown in Figure 6, where A_V is the amplitude in the V -band. Also shown are the RR Lyrae stars in 14 OoII-type GCs (NGC 4590, NGC 5053, NGC 7078, ω Cen, NGC 5466, NGC 6426, NGC 6333, NGC 6341, NGC 5024, NGC 7089, NGC 2419, NGC 5286, NGC 6101 and NGC 1904). The period- A_V relation for OoI and OoII clusters is overplotted, where the fundamental-mode and first-overtone PA relations are derived from the M3 RRL (Cacciari et al. 2005).

The M22 RR0 variables occupy the area of the PA diagram where OoII-type variables tend to lie (e.g., Clement & Shelton 1999). Unlike RR0 variables, RR1 variables are not expected to follow a roughly linear sequence in the PA diagram (e.g., Bono et al. 1997), and this is clearly seen within the RR1 population of M22. The “hairpin” shape predicted for the RR1 variables in the theoretical PA diagram is evident, albeit with significant outliers. The approximate relation

$$A_V = -9.75 + 57.3P - 80P^2 \quad (4)$$

is derived from the M22 RR1 variables. Blazhkocity can affect the position of a star on the PA diagram (e.g., Cacciari et al. 2005) and as discussed above, some of the RR Lyrae stars in M22 may exhibit signs of this phenomenon. The amount of the amplitude change due to the Blazhko effect is no more than ~ 0.1 mag in V (see Figure 2), which does not significantly affect the location of the star in the PA diagram.

Amplitude ratios are often used both to identify variables that might have their photometry compromised by faint companions and to classify variable stars, especially the low amplitude RR Lyrae variables. In light of this, the ratios of the RR0 and RR1 amplitudes in the differ-

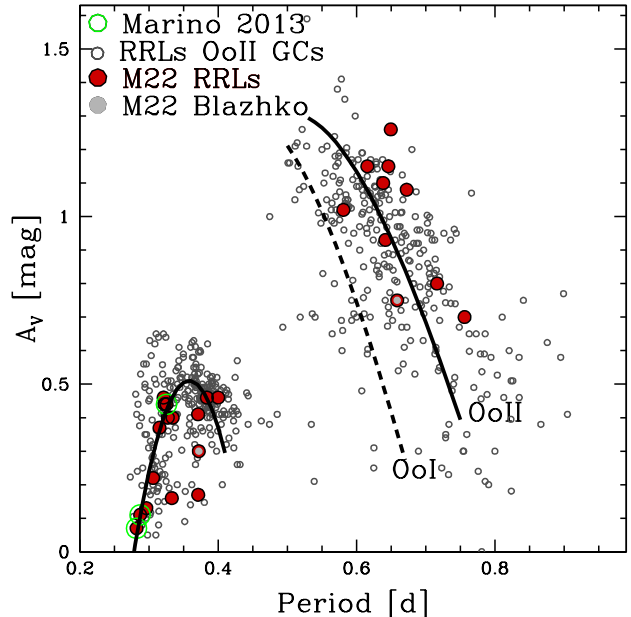


FIG. 6.— Position of the M22 RR Lyrae stars on the period- A_V diagram. The stars exhibiting Blazhkocity are represented by gray circles. The dashed line is typical for RR0 variables in OoI clusters and the solid line is for OoII clusters, according to Cacciari et al. (2005). The periods and V -band amplitudes for RR Lyrae stars in 14 OoII-type GCs are also shown by small circles (see text for details).

ent bands are given in Table 3 and Table 4. We have excluded the RR0 star KT-55 in the amplitude ratio determination, as it has an uncertain A_I (see Table 2). Similarly, the RR1 stars NV2, NV3 and V18 are not included in the amplitude ratios due to no/uncertain A_B and A_I s. The amplitude ratios of the RR Lyrae stars in few Galactic GCs are also listed for comparison purposes and plotted as a function of their period in Figure 7. There is a scatter of ~ 0.2 mag for A_B/A_I and A_V/A_I , but a much smaller scatter of ~ 0.05 mag, for A_B/A_V . Moreover, Kuehn et al. (2011) find $A_B/A_V = 1.28 \pm 0.02$ from 26 RR Lyrae variables in the OoI-type LMC GC NGC 1466 (see their Figure 9), and Kinman & Brown (2010) find $A_B/A_V = 1.27$ from 12 field RR Lyrae stars in the Northern Sky Variability Survey (NSVS) data. These results are in excellent agreement with the A_B/A_V amplitude ratios obtained here and in other Galactic GCs. This may suggest that Galactic field and cluster RR Lyrae and cluster LMC RR Lyrae stars have A_B/A_V RR Lyrae amplitude ratios that are independent of their host system.

3.5. RR Lyrae Reddenings

The interstellar extinction toward M22 is high ($E(B-V) = 0.34$ mag; 2010 edition of Harris 1996) and variations of reddening are expected within the field of view of M22 (e.g., Monaco et al. 2004; Piotto et al. 2012). Minimum-light colors of the RR0 Lyrae variables have been used as a tool for measuring the interstellar reddening toward RRLs (Sturch 1966; Walker 1990; Blanco 1992; Mateo et al. 1995; Kunder et al. 2010). Sturch (1966) derived a formula to determine reddenings toward RR Lyrae stars using their $(B-V)$ colors at minimum light, which was then corrected to be on the GC

TABLE 3
EMPIRICAL AMPLITUDE RATIOS OF THE RR0 LYRAE VARIABLES

| cluster | A_U/A_I | A_B/A_I | A_V/A_I | A_B/A_V | num stars | source |
|----------|-----------------|-----------------|-----------------|-----------------|-----------|-----------|
| M22 | 1.89 ± 0.05 | 2.09 ± 0.04 | 1.66 ± 0.03 | 1.26 ± 0.02 | 9 | this work |
| NGC 3201 | – | 1.88 ± 0.04 | 1.49 ± 0.03 | 1.26 ± 0.02 | 56 | (1) |
| NGC 1851 | – | 2.00 ± 0.04 | 1.57 ± 0.02 | 1.27 ± 0.02 | 19 | (2) |
| NGC 4147 | – | 2.19 ± 0.24 | 1.74 ± 0.25 | 1.29 ± 0.12 | 5 | (3) |
| NGC 4590 | – | 2.03 ± 0.04 | 1.55 ± 0.03 | 1.31 ± 0.01 | 12 | (4) |
| NGC 7078 | – | 1.93 ± 0.05 | 1.58 ± 0.04 | 1.23 ± 0.01 | 25 | (5) |
| NGC 6715 | – | 1.89 ± 0.05 | 1.53 ± 0.03 | 1.25 ± 0.03 | 40 | (6) |

TABLE 4
EMPIRICAL AMPLITUDE RATIOS OF THE RR1 VARIABLES

| cluster | A_U/A_I | A_B/A_I | A_V/A_I | A_B/A_V | num stars | source |
|----------|-----------------|-----------------|-----------------|-----------------|-----------|-----------|
| M22 | 1.83 ± 0.10 | 2.17 ± 0.07 | 1.61 ± 0.07 | 1.37 ± 0.06 | 13 | this work |
| NGC 3201 | – | 1.97 ± 0.02 | 2.05 ± 0.07 | 1.02 ± 0.04 | 4 | (1) |
| NGC 1851 | – | 2.04 ± 0.08 | 1.63 ± 0.05 | 1.25 ± 0.02 | 8 | (2) |
| NGC 4147 | – | 2.06 ± 0.14 | 1.54 ± 0.25 | 1.38 ± 0.18 | 10 | (3) |
| NGC 4590 | – | 2.10 ± 0.02 | 1.62 ± 0.02 | 1.30 ± 0.01 | 16 | (4) |
| NGC 7078 | – | 1.97 ± 0.06 | 1.55 ± 0.04 | 1.28 ± 0.03 | 13 | (5) |
| NGC 6715 | – | 1.7 ± 0.1 | 1.56 ± 0.02 | 1.08 ± 0.08 | 8 | (6) |

(1) Layden & Sarajedini (2003); (2) Walker (1998); (3) Stetson (2005); (4) Walker (1994); (5) Corwin et al. (2008); (6) Sollima et al. (2010)

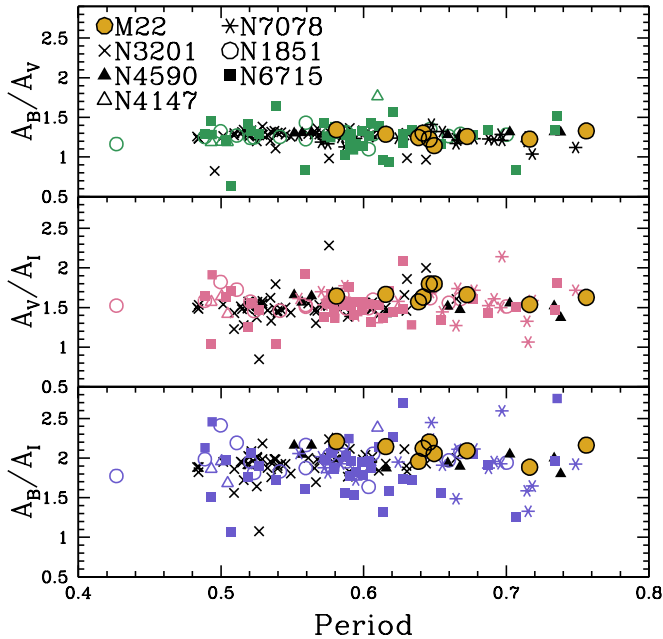


FIG. 7.— The RR Lyrae amplitude ratios as a function of period for seven Milky Way globular clusters (see Table 3).

scale by Walker (1990). In particular, for RR0 variables, Walker (1990) obtained:

$$E(B-V) = (B-V)_{min} - 0.24 P - 0.056 [\text{Fe}/\text{H}]_{\text{ZW84}} - 0.336 \quad (5)$$

where $(B-V)_{min}$ is the color at minimum light (phase between 0.5 and 0.8), P is the period in days and

TABLE 5
REDDENING DETERMINATIONS FROM RR LYRAE VARIABLES IN M22

| Name | $(B-V)_{min}$ | $E(B-V)^b$ | $(V-I)_{min}$ | $E(V-I)$ |
|------------------|-----------------|------------|-----------------|----------|
| V1 | 0.80 ± 0.01 | 0.41 | 1.08 ± 0.01 | 0.50 |
| V2 | 0.77 ± 0.01 | 0.38 | 1.02 ± 0.02 | 0.44 |
| V4 | 0.79 ± 0.01 | 0.38 | 1.07 ± 0.01 | 0.49 |
| V6 | 0.78 ± 0.01 | 0.39 | 1.01 ± 0.02 | 0.43 |
| V7 | 0.76 ± 0.01 | 0.37 | 1.05 ± 0.01 | 0.47 |
| V10 | 0.76 ± 0.01 | 0.37 | 1.05 ± 0.01 | 0.47 |
| V13 | 0.73 ± 0.01 | 0.33 | 0.98 ± 0.01 | 0.40 |
| V20 | 0.79 ± 0.01 | 0.37 | 1.07 ± 0.02 | 0.49 |
| V23 ^a | 0.85 ± 0.04 | 0.38 | 1.10 ± 0.02 | 0.52 |
| KT-55 | 0.80 ± 0.01 | 0.40 | 1.07 ± 0.01 | 0.49 |

^a Based on a light curve using data only from runs 9, 14, and 16, which had minimal scatter.
^b from Equation 5

$[\text{Fe}/\text{H}]_{\text{ZW84}}$ is the metallicity in the Zinn & West (1984) scale. Similarly, using the V and I passbands, Guldenschuh et al. (2005) find:

$$E(V-I) = (V-I)_{min} - 0.58 \pm 0.02 \quad (6)$$

and that this relation is largely independent of period, amplitude and metallicity.

The observed $B-V$ and $V-I$ color at minimum light is calculated using the best-fit light-curve templates and listed in Table 5. Comparing colors at minimum light derived from fitted template light curves, to minimum-light colors estimated directly from the observation, we find that the values agree usually to within 0.01 mag. The average $E(B-V)$ from Equation 5, adopting $[\text{Fe}/\text{H}]_{\text{ZW84}} = -1.73$ dex (which is $[\text{Fe}/\text{H}] = -1.75$ on the Kraft & Ivans 2003, scale), gives $E(B-V) = 0.38 \pm 0.02$ mag. The average $E(V-I)$ from Equation 6 is 0.47 ± 0.03 mag which translates to $E(B-V)$ of $0.34 - 0.37$ mag, depending on the reddening law used.¹⁵ Adopting an average $E(V-I)/E(B-V)$ ratio of 1.35, $E(B-V)$ is 0.35 ± 0.04 mag.

The average of the $E(B-V)$ values from Equation 5 and Equation 6 is $E(B-V) = 0.36 \pm 0.03$, in excellent agreement with the value of $E(B-V) = 0.38 \pm 0.04$ from Monaco et al. (2004) and Richter et al. (1999). Older reddening estimates range from $E(B-V) = 0.32$ to 0.42 (Hesser 1976; Harris & Racine 1979; Crocker 1988). Monaco et al. (2004) find that differential reddening in M22 is $\Delta E(B-V) \sim 0.06$, and our values of $E(V-I)$ and $E(B-V)$ show a similar range.

Walker (1998) showed that the blue edge of the instability strip in GCs appears to have a constant $B-V$ over a wide range of metallicity, with $(B-V)_{0,FBE} = 0.18 \pm 0.01$. The blue edge of our sample is estimated by averaging the $B-V$ color of the five bluest RR Lyrae stars and the five reddest constant stars. (Because measurement uncertainties guarantee observational tails beyond true limits, scissoring these two samples largely cancels out the systematic error that would arise if we had used the most extreme $B-V$ RR Lyrae to define an envelope.) Hence the blue edge of the IS is $B-V = 0.53$ mag, suggesting $E(B-V) = 0.35 \pm 0.01$. This color excess is in excellent agreement with that found from the RR Lyrae

¹⁵ Different values for the transformation from $E(V-I)$ to $E(B-V)$ include a $E(V-I)/E(B-V)$ ratio of 1.4 (Schlegel et al. 1998; Schlafly & Finkbeiner 2011), 1.35 (McCall 2004) and 1.28 (Cardelli et al. 1989, 1992).

minimum light colors.

4. THE COLOR-MAGNITUDE DIAGRAM

The color-magnitude diagram for M22 is shown in Figure 8, in V versus $V-I$ and $U-I$, where the CMD is cleaned using the proper motions provided by Zloczewski et al. (2013). About 13% of GCs in the Milky Way (15 out of 114) have strong extended HBs (E-BHBs), a feature which may be due to the presence of helium-enhanced second-generation subpopulations (e.g., Norris 2004; Piotto et al. 2005; Lee et al. 2007). It has also been shown that E-BHB GCs are in general more massive than normal GCs and have different kinematics (e.g., Lee et al. 2007). This suggests that GCs with and without E-BHBs have different origins. M22 is known to have a strong E-BHB, and with our proper motion cleaned HB and accurate, calibrated photometry, we easily see that the E-BHB reaches 1.5 magnitudes fainter than the V -magnitude main-sequence turnoff at its high temperature end.

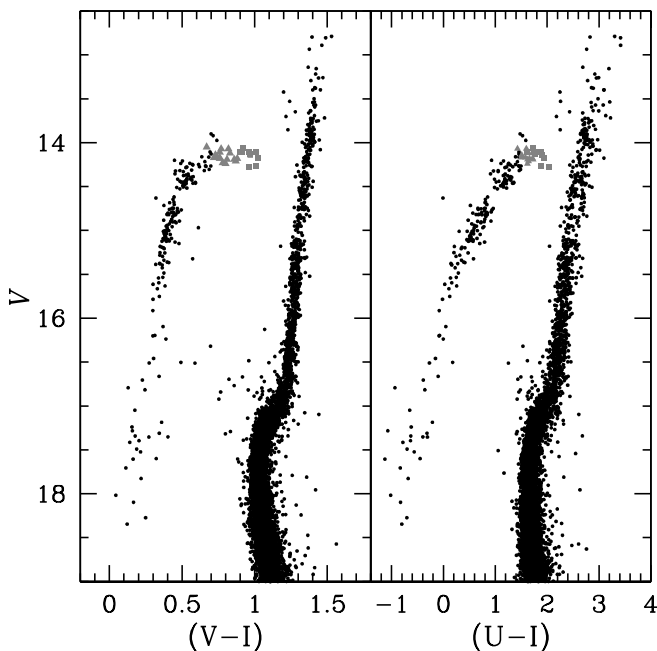


FIG. 8.— The M22 color-magnitude diagram, showing the location of the RR Lyrae variable stars in gray.

4.1. HB morphology parameters

Most key HB morphology parameters compare the number ratios of stars in different parts of the HB (e.g., Mironov 1972; Buonanno 1993; Lee et al. 1994), with one of the most frequently used HB morphology parameters defined as $(B-R)/(B+V+R)$ (see Lee et al. 1994). This requires the knowledge of the number of blue (B) stars (bluer than the RR Lyrae gap), variable (V) and red (R) HB stars (number of HB stars redder than the gap) in a cluster. For M22, R is zero and V is 26, as determined in §4. An estimate of the number of BHB, however, is complicated by the many field stars near M22. The proper motion cleaned HB ensures that the stars are cluster members, but again due to the heavy crowding of the field, the proper motion completeness is about 50 per cent (Zloczewski et al. 2013).

Figure 9 shows the observed star counts as a function of radial distance, and shows the logarithm of star counts plotted against apparent magnitude. If we can assume that the completeness is the same for all magnitude bins beyond some radius, say for instance 4 arcminutes, this can be interpreted as a luminosity function for that radial zone, at least. The radial zone that will be the most incomplete is the innermost radial zone, where the crowding is most severe, and in the case of the Zloczewski et al. (2013) proper motion cleaned catalog, also the outermost radial zone, where the fraction of the annulus contained within the rectangular field of view diminishes. The star counts of the outermost two zones can be compared (e.g., at 6' and at 7'), and a similar magnitude distribution would indicate they are comparably complete. Where the magnitude distribution begins to diverge is where a radial zone is beginning to be incomplete. In this way, the onset of where incompleteness sets in as a function of radial distance from the cluster center is mapped (see also Walker et al. 2011).

For the magnitude range of the HB, from $V\sim 15$ to $V\sim 18.5$ mag, there is no divergence in the apparent magnitude distribution from $r\sim 4-6'$ in the Zloczewski et al. (2013) sample. The number of HB stars from the Zloczewski et al. (2013) proper-motion selected stars between $r=4'$ and $r=6'$ is thirty-two, and the number of proper-motion selected RR Lyrae stars in this same range is zero. Therefore, $(B:V:R) = (32 \pm 6 : 0 \pm 1 : 0 \pm 1)$, or $(B-R)/(B+V+R) = +1.0 \pm 0.1$.

This same procedure is repeated with the sample of stars from our M22 photometric catalog. Figure 9 shows that there is little or no sign of incompleteness at distances between $r=4'$ and $r=8'$. In this radial zone there are 147 blue HB stars, 5 RR Lyrae stars and 0 red HB stars, giving a $(B:V:R) = (64 \pm 12 : 2 \pm 2 : 0 \pm 1)$ or $(B-R)/(B+V+R) = +0.97 \pm 0.1$ in agreement with what was obtained from the proper motion cleaned sample.

A comparison of the HB-type of M22 with respect to other GCs that harbor a population of RR Lyrae variables is shown in Figure 10, where the HB-type comes from the compilation of Catelan (2009). As expected, M22 has a [Fe/H], HB-type and Oosterhoff classification consistent with an old halo GC.

4.2. Gaps on the Blue HB

Rood & Crocker (1985, 1989) suggest that a good method for analyzing the distribution of stars along the HB is to define a coordinate, l_{HB} , which is linear along the HB ridge-line. Briefly, the length of the HB ridge-line is divided into equal bins, and the number of stars populating each bin (perpendicular to the ridge-line) is determined (see bottom of Figure 11). Although l_{HB} has been used frequently (e.g., Ferraro et al. 1992; Dixon et al. 1996; Catelan et al. 1998), it has been given different definitions (i.e., different bin sizes along the HB ridgeline), making it difficult to accurately reproduce and compare from cluster to cluster. In response to such confusion, Piotto et al. (1999) outline a recipe to obtain a “standard” l_{HB} , and their procedure is adopted here.

The l_{HB} distribution is shown in Figure 11, using the proper motion cleaned HB stars as well as the RR Lyrae stars in the cluster. The l_{HB} distribution is asymmetric; that the stellar distribution along the HB is not symmetric is a feature characteristic of blue HB clusters. The

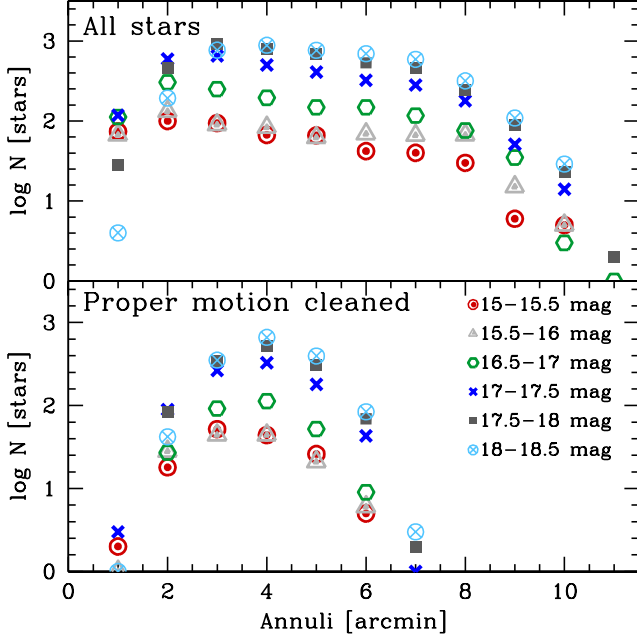


FIG. 9.— *Bottom*: The number of stars per radial zone for the proper-motion selected M22 population. The different symbols represent different V magnitudes bins, which are specified in the top right-hand corner. *Top*: The number of stars per radial zone for our complete sample of stars.

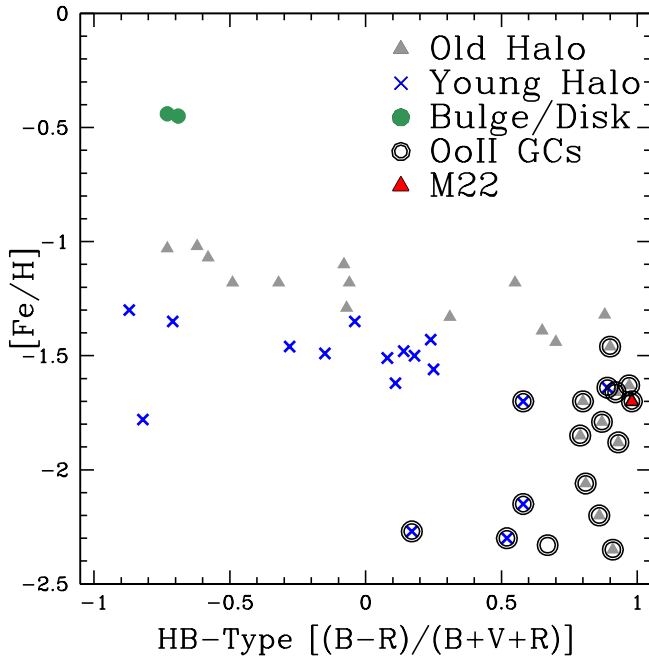


FIG. 10.— Position of the Galactic globular clusters with a defined Oosterhoff type in the metallicity–“HB type” plane. The bulge/disk, old halo and young halo clusters, as defined by Mackey & van den Bergh (2005), are labeled.

main feature of the l_{HB} is a double peaked distribution, one peak at $l_{HB}=26$ and another at $l_{HB}=21$. Between the two peaks is a pronounced gap, at $l_{HB}=23$, clearly seen at $V=14.6$, and first noted by Cho et al. (1998). To our knowledge, this is the first time that a gap clearly

shows up in the middle of the so-called hot HB stars.

Unfortunately, it is difficult to tie physical parameters (such as T_{eff} or mass) to any gaps or over-densities along the HB from the l_{HB} parameter. This is because the HB ridge line does not follow the ZAHB, whereas theoretical models do. We have therefore used the ZAHB shown in Figure 5 to estimate the temperature of where this gap occurs. In particular, the ZAHB with a normal CNO and $[Fe/H]=-1.84$ dex is used, as that has spectroscopically been shown to be appropriate for the M22 HB (Marino et al. 2013). From $(V-I, V)=(0.44, 14.53)$ to $(V-I, V)=(0.41, 14.71)$, which is the approximate range of the “gap” in a V versus $V-I$ (see Figure 8), the T_{eff} runs from 9,500 K to 10,500 K. Therefore, the HB gap in M22 is on the cool side of the Grundahl et al. (1998) “jump”, which is seen in the UV CMDs of E-BHB GCs at $T_{eff}^{jump}=11,500 \pm 500$ K (e.g., Grundahl et al. 1999).

A peak at $l_{HB}=26$ is also seen in NGC 6273 (Piotto et al. 1999), suggesting that there may be some preference for stars to clump here, although a sample of two clusters is not sufficient to draw any conclusions at this point.

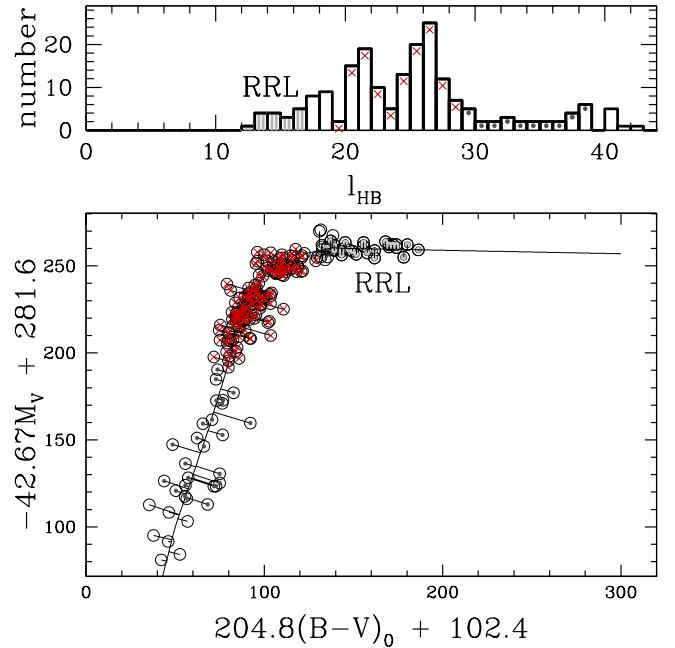


FIG. 11.— *Bottom*: The projection of the proper motion cleaned HB stars of M22 onto the HB ridge-line, with the adopted ridge-line and projection vector of each star shown. Using this scale, one unit in the abscissa has the same length as one unit in the ordinate (see Piotto et al. 1999, for details). At $204.8(B-V)_0 + 102.4 = 300$ is the adopted zero point for l_{HB} and corresponds to $B-V = 0.965$. Different symbols indicate the RR Lyrae variables, as well as the stars with $l_{HB} = 0, 10, 20, 30, 40$ along curve. *Top*: The observed distribution of stars along the HB.

4.3. Radial Distribution

The currently available models for the formation of multiple populations in a GC suggest that the second generation stars should form in the inner regions of the cluster, shortly after the ejecta from the more massive first generation stars accumulated there and subsequently mixed with pristine, unpolluted matter (e.g.,

D’Ercole et al. 2008; Decressin et al. 2010). This is actually observed in the case of the not-yet dynamically relaxed GCs ω Cen and M13 (Sollima et al. 2007; Bellini 2009; Lardo et al. 2011; Johnson & Pilachowski 2012). Despite these cases, it is believed that the majority of the MW GCs will have the presence of radial stellar population gradients erased as a consequence of the long-term dynamical evolution occurring during the last ~ 12 Gyr of their life (e.g., as it seems is the case for the GC NGC 1851; Milone et al. 2009).

That M22 has a double RGB with different Ca abundances has been shown from by Lee et al. (2009) from the hk index of the $Ca\text{-}by$ photometry. Joo & Lee (2013) also use Strömberg photometry to show that the RGB consists of two stellar populations. In Figure 12 we use the V vs $c_{U,B,I}$ diagram, where $c_{U,B,I} = (U-B)-(B-I)$, to separate the blue and red RGB stars. Here, the red RGB stars are arbitrarily defined as those with $c_{U,B,I} < -2.26$ and the blue RGB stars have $c_{U,B,I} > -2.26$. The $c_{U,B,I}$ index was introduced by Monelli et al. (2013) and maximizes the separation among stars with different helium and light-elements content. This is because the $U-B$ color is sensitive to light-element variations (Marino et al. 2008; Sbordone et al. 2011) and the $B-I$ color is very efficient in disentangling stellar populations with different helium abundance (Piotto et al. 2007; di Criscienzo et al. 2011). The radial distributions of the blue and red RGB stars are shown in the top panel of Figure 12. and suggests that the red population is slightly more centrally concentrated than the blue RGB population. This is also confirmed from the results of a two-sided KS test, which indicates that the red and blue RGB stars trace the same radial distribution with KS-prob = 0.10. Such a KS-prob is just marginally greater than the default threshold KS-prob = 0.05 below which one rejects the null hypothesis.

Similarly, Marino et al. (2012a) present an abundance analysis of 101 SGB stars in M22, finding that the faint SGB is populated by more metal-rich stars than the bright SGB. Marino et al. (2012a) classify their SGB stars as s -poor and s -rich based on the spectroscopic C, Sr and Ba abundances, and the cumulative radial distribution of their sample of SGB stars (their Table 3) is shown in Figure 13. Although the sample is small, the s -poor and s -rich stars appear to have different radial distributions beyond ~ 3 arc minutes. The result of a two-sided KS test indicates that the faint SGB and bright SGB stars trace the same radial distribution with KS-prob = 0.19 beyond a radius of 3 arc minutes.

The faint SGB evolves in a redder RGB sequence whereas the brighter SGB evolves in a bluer branch. Both the RGB (red/blue) and SGB (bright/faint) populations show hints of radial trends, but ultimately, cleaner and larger samples are needed to make firm conclusions of the long-term dynamical evolution of M22.

In general, GCs with strong E-BHBs, as seen in the HB of M22, are modeled by helium-enhanced second-generation subpopulations (e.g., Norris 2004; Piotto et al. 2005; Lee et al. 2007). As the second generation of stars in M22 can be distinguished radially, as shown clearly with the M22 SGB and RGB stars, it is of interest to use radial plots to search for trends in the stars along the HB.

Figure 14 shows the radial distribution of the E-BHB

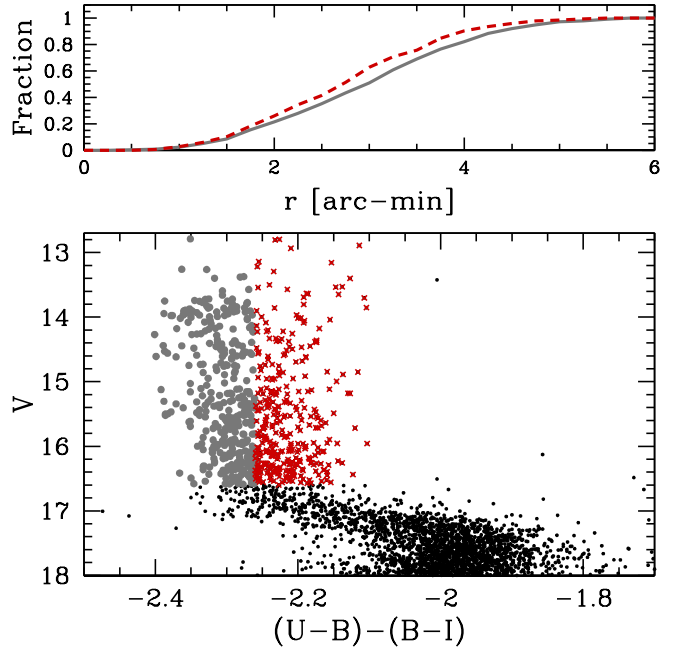


FIG. 12.— The RGB of M22 in the V vs. $c_{U,B,I}$ diagram, where $c_{U,B,I} = (U-B)-(B-I)$ is sensitive to stellar helium and light element content. The grey and red points are arbitrarily divided at $c_{U,B,I} = 2.26$ to separate blue and red RGB stars, respectively. (Top): The cumulative radial distributions of red RGB (dashed curve) and blue RGB stars (solid curve).

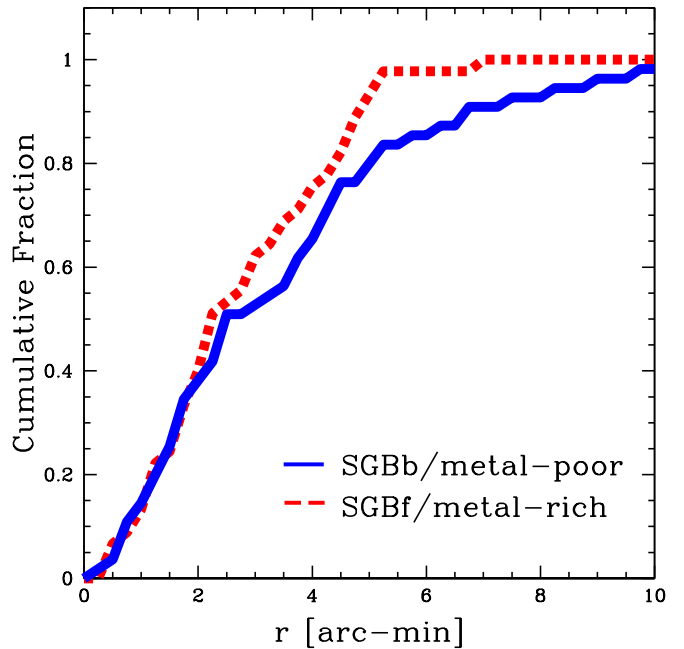


FIG. 13.— Normalized cumulative distribution of the Marino et al. (2012a) sample of SGBb and SGBf stars as a function of distance from the cluster center.

stars, using our photometry and also using the proper-motion selected stars from Zloczewski et al. (2013). We limit our analysis to the stars at distances between $r=4'$ and $r=6'$ and to $V=18.0$ mag, as we believe that this is the range where these samples show no magnitude bias

(see Figure 9 and discussion). Both our sample and the Zloczewski et al. (2013) sample show that the E-BHB stars can not be distinguished from the rest of the HB stars in a radial plot. Unfortunately, the number of HB stars in the outer parts of M22 is significantly smaller than the number of stars closer to the central part of the cluster. For example, there are only 36 E-BHB stars in our sample at distances larger than $r=4'$ from the cluster center. Therefore the significance of this finding might be somewhat biased. If confirmed, however, this would indicate that the most extreme BHB stars in M22 are formed alongside the reddest part of the HB. Because Marino et al. (2013) have shown that the reddest HB stars belong to the first generation of stars, this would then also suggest that the E-BHB stars in M22 belong to the first generation and are not He enhanced.

Our result of no strong radial separation of the HB components in M22 is in agreement with that found in the globular cluster NGC 2808 (Iannicola et al. 2009). They divide the NGC 2808 HB stars into three radial bins, and find that the relative fractions of cool, hot, and extreme HB stars do not change when moving from the center to the outskirts of the cluster. It was also found from high resolution spectra of hot HB stars in ω Cen, that a significant fraction of E-BHB stars are helium-poor (Moehler et al. 2011). They find that among the hottest stars in the E-BHB (in the temperature range 30 000 K to 50 000 K), $\sim 30\%$ are actually helium-poor.

Our result is also in agreement with some of the M22 population models presented by Joo & Lee (2013) (see their Figure 13). For example, Joo & Lee (2013) show that if there is a difference in $[\text{CNO}/\text{Fe}]$ between the two SGB M22 subpopulations, as suggested for NGC 1851 (Cassisi et al. 2008; Salaris et al. 2008), both the E-BHB and the reddest HB will have a roughly equal mix of first and second generation stars. Additional theoretical models by Moehler et al. (2011) have shown that the presence of E-BHB stars can be explained as having formed by an independent evolutionary channel: hot helium flashers and a significant fraction of E-BHB stars may come from the above channel. Therefore, here we present additional observational results in contradiction to the generally accepted view on the formation of an E-BHB (e.g., Norris 2004; Piotto et al. 2005; Lee et al. 2007; D’Antona & Caloi 2008). Especially in this regard, radial studies involving wide-field photometry on a large sample of E-BHB clusters would be a worthwhile endeavor.

5. CONCLUSIONS

The first calibrated *UBVI* photometry is presented for 26 RR Lyrae variables in the chemically heterogeneous, split-SGB globular cluster NGC 6656 (M22). Four of these variables are newly discovered, which increases the specific RR Lyrae fraction of M22 to $S_{RR}=10.4$ where $S_{RR} = N_{RR} \times 10^{0.4(7.5+M_V)}$, and $M_V=-8.50$ (Harris 1996, 2010 update) is the cluster’s integrated absolute magnitude in *V*. The pulsational parameters of the variables suggest that 10 RR Lyrae variables are fundamental-mode pulsators with mean periods of $\langle P_0 \rangle = 0.66 \pm 0.02$ days and 16 are first-overtone variables with mean periods of $\langle P_1 \rangle = 0.33 \pm 0.01$ days. The number ratio of the RR1-type variables to the total number of the RRL-type variables is $N_1/N_{RR} = 0.61$. Therefore M22

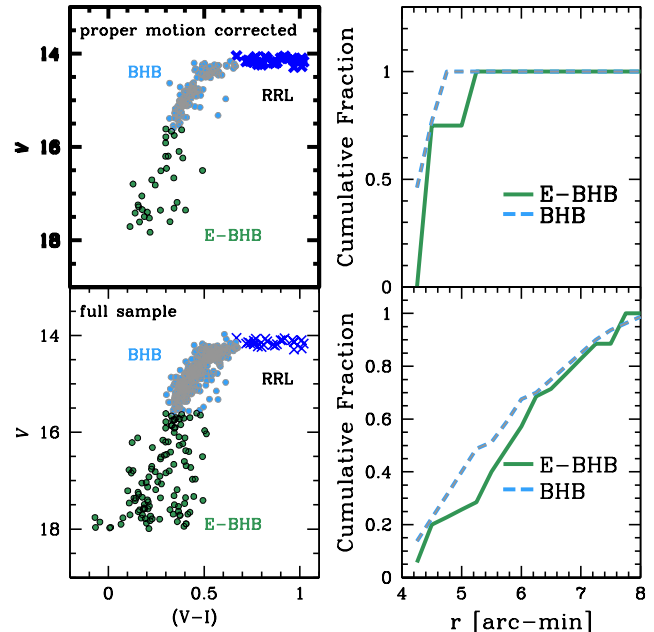


FIG. 14.— Normalized cumulative distribution of the E-BHB stars and the BHB stars as a function of distance from the cluster center.

can be classified as an OoII cluster, which is expected considering the metallicity and horizontal branch morphology of the cluster.

The mean magnitude for the RRLs is $m_{V,RR} = 14.15 \pm 0.02$ mag, and the reddening from their minimum light colors was determined to be $E(B-V)=0.36 \pm 0.02$ mag, in agreement with previous studies (e.g., Monaco et al. 2004; Richter et al. 1999). Using both the recent recalibration of the RR Lyrae luminosity scale by Catelan & Cortés (2008) and the quadratic relation between RR Lyrae absolute magnitude and metallicity from Bono, Caputo, & di Criscienzo (2007), the RR Lyrae variables have absolute magnitudes of $M_V=0.57 \pm 0.13$. This leads to an RR Lyrae distance of $(m-M)_{V,RRL}=13.58 \pm 0.13$ and adopting $E(B-V)=0.36$ mag, $(m-M)_{0,RRL}=12.46 \pm 0.13$ mag. We note, however, that a 70% brighter M_V is found when using the Benedict et al. (2011) $M_V-[\text{Fe}/\text{H}]$ relation, which would change the RR Lyrae distance modulus by ~ 0.2 mag. A somewhat brighter M_V is in accordance to the distance determination of $(m-M)_V=13.65$ mag found by using theoretical Zero Age Horizontal Branch loci and accounting for the most recent spectroscopic analysis of the chemical composition of the cluster stars.

From the comparison of theoretical ZAHB sequences with observations, we find that most RRLs have a mass of $M=0.64-0.68M_{\odot}$ if there is no non-canonical enhancement of CNO elements or helium. If such non-canonical enhancement is present, the mass range could be more like $0.60-0.61M_{\odot}$. We also find that, theoretically, if two populations of RR Lyrae variables existed in M22 with abundance ratios similar to the two populations of SGB stars (e.g., Marino et al. 2012a), it would be very difficult to distinguish between the more metal-rich and more metal-poor variables from their luminosities alone. This is because the *s*-rich stars have higher C and N contents,

so their luminosities would be comparable to the more metal-poor variables.

After correcting for completeness on the horizontal branch, $(B-R)/(B+V+R)=+0.97\pm 0.1$ is obtained. This is one of the largest HB values for a GC with a substantial population of RR Lyrae stars, and combined with its $[\text{Fe}/\text{H}]$ and Oosterhoff type, is consistent with the classification of an old halo GC.

Different spatial distributions can be separated in the Marino et al. (2012a) sample of SGB stars as well as in the RGB, with the more metal-rich SGBf and the redder RGB being marginally more centrally concentrated than the SGBb and bluer RGB. Therefore a search of different radial distributions in the HB stars has been carried out. Although the E-BHB stars are usually explained as being a helium-enhanced second-generation subpopulation (e.g., Norris 2004; Piotto et al. 2005; Lee et al. 2007), we are not able to radially distinguish the E-BHB from the rest of the stars on the horizontal branch. This may mean that the E-BHB stars are not exclusively a second-generation subpopulation, as also seen with the E-BHB of NGC 2808 (Iannicola et al. 2009) and the E-BHB of ω Cen (Moehler et al. 2011). However, the small numbers of E-BHB stars at large cluster radii limit the significance of this interpretation.

Combining our photometry with the proper-motion cleaned sample by Zloczewski et al. (2013), we find at least one “gap” and two over-densities on the blue HB. Although the gap is located in an unusual part of the HB, at $V=14.6$ mag and in the middle of the so-called hot HB stars, the over-density at $l_{HB}=26$ is also seen in NGC 6273 (Piotto et al. 1999), suggesting that there may be some preference for stars to clump here.

This research uses services or data provided by the NOAO Science Archive. NOAO is operated by the Association of Universities for Research in Astronomy (AURA), Inc. under a cooperative agreement with the National Science Foundation. This research is also based on observations obtained at the Southern Astrophysical Research (SOAR) telescope, which is a joint project of the Ministério da Ciência, Tecnologia, e Inovação (MCTI) da República Federativa do Brasil, the U.S. National Optical Astronomy Observatory (NOAO), the University of North Carolina at Chapel Hill (UNC), and Michigan State University (MSU). G.B. thanks ESO for support as a science visitor. This work was partially supported by PRIN-INAF 2011, (P.I.: M. Marconi) and by PRIN/MIUR (2010LY5N2T), (P.I.: F. Matteucci). J.-W.L. acknowledges financial support from the Basic Science Research Program (grant No. 2010-0024954) and the Center for Galaxy Evolution Research through the National Research Foundation of Korea. Support for M.C. is provided by the Chilean Ministry for the Economy, Development, and Tourism’s Programa Iniciativa Científica Milenio through grant P07-021-F, awarded to The Milky Way Millennium Nucleus; by the BASAL Center for Astrophysics and Associated Technologies (PFB-06); by Proyecto Fondecyt Regular #1110326; and by Proyecto Anillo ACT-86.

REFERENCES

- Alves-Brito, A., Yong, D., Meléndez, J., Vásquez, S., Karakas, A. I. 2012, *A&A*, 540, 3
- Anderson, J., Cool, A., King, I. R. 2003, *ApJ*, 597, L137
- Arellano Ferro, A., Bramich, D. M., Figuera Jaimes, R., Giridhar, S., & Kuppuswamy, K. 2012, *MNRAS*, 420, 1333
- Bailey, S. I. 1902, *Harv. Ann.*, 38
- Bellazzini, M., Ibata, R. A., Chapman, S. C., et al. 2008, *AJ*, 136, 1147
- Bellini, A., Piotto, G., Bedin, L. R., King, I. R., Anderson, J., Milone, A. P. & Momany, Y. 2009, *A&A*, 507, 1393
- Benedict, G. F., McArthur, B. E., & Feast, M. W. et al. 2011, *AJ*, 142, 187
- Benkő, J. M., Kolenberg, K., Szabó, R. et al. 2010, *MNRAS*, 409, 1585
- Blanco, V. 1992, *AJ*, 104, 734
- Blazhko, S. 1907, *Astr. Nachr.*, 175, 325
- Bono, G., Caputo, V., Castellani, V., & Marconi, M. 1997, *A&AS*, 121, 327
- Bono, G., Caputo, F., di Criscienzo, M. 2007, *A&A*, 476, 779
- Buchler, R.J. & Kolláth, Z. 2011, *ApJ*, 731, 24
- Butler, D., Kraft, R.P., Miller, J.S. & Robinson, L.B. 1973, *ApJ*, 179, 73
- Buonanno, R. 1993, in *ASP Conf. Proc.* 48, *The Globular Cluster-Galaxy Connection*, ed. G. H. Smith & J. P. Brodie (San Francisco: ASP), 131
- Cacciari, C., Corwin, T. M., & Carney, B. W. 2005, *AJ*, 129, 267
- Cardelli, J. A., Sembach, K. R., & Mathis, J. S. 1992, *AJ*, 104, 1916
- Cardelli, J.A., Clayton, G.C. & Mathis, J.S. 1989, *ApJ*, 345, 245
- Carretta, E., & Gratton, R. G. 1997, *A&AS*, 121, 95
- Carretta, E., Bragaglia, A., Gratton, R. & Lucatello S. 2009a, *A&A*, 505, 117
- Carretta, E., Bragaglia, A., Gratton, R. & Lucatello S. 2009b, *A&A*, 505, 139
- Carretta, E., Bragaglia, A., Gratton, R. G., et al. 2010a, *ApJ*, 714, L7
- Carretta, E., Gratton, R. G., Lucatello, S. et al. 2010b, *ApJ*, 722, L1
- Cassisi, S., Potekhin, A.Y., Pietrinferni, A., Catelan, M. & Salaris, M. 2007, *ApJ*, 661, 1094
- Cassisi, S., Salaris, M., Pietrinferni, A., Piotto, G., Milone, A. P., Bedin, L. R., & Anderson, J. 2008, *ApJ*, 672, L115
- Catelan, M., Borissova, J., Sweigart, A.V. & Spassova, N. 1998, *ApJ*, 494, 265
- Catelan, M., Pritzl, B.J., & Smith, H.A. 2004, *ApJS*, 154, 633
- Catelan, M. & Cortés, C. 2008, *ApJ*, 676, L135
- Catelan, M. 2009, *Ap&SS*, 320, 261
- Cho, D.H., Lee, S.-W. & Sung, H. 1008 *JKAS*, 31, 67
- Clement, C.M. & Walker, I.R. 1991, *AJ*, 101, 1352
- Clement, C.M. & Shelton, I. 1999, *ApJ*, 515, L85
- Clement, C.M. et al. 2001, *AJ*, 121, 2587
- Clementini, G., Raffaele, G., Bragaglia, A., Carretta, E., Di Fabrizio, L & Maio, M. 2003, *AJ*, 125, 1309
- Cohen, J.G., Kirby, E.N., Simon, J.D. & Geha, M. 2010, *ApJ*, 725, 288
- Corwin, T.M., Catelan, M., Smith, H.A., Borissova, J., Ferraro, F.R. & Raburn, W.S. 2003, *AJ*, 125, 2543
- Corwin, T.M., Borissova, J., Stetson, P.B. et al. 2008, *AJ*, 135, 1459
- Crocker D. A., 1988, *AJ*, 96, 1649
- Crocker, D. A., Rood, R. T., & O’Connell R.W. 1988, *ApJ*, 332, 236
- D’Antona, F. & Caloi, V. 2008, *MNRAS*, 390, 693
- D’Ercole, A., Vesperini, E., D’Antona, F., McMillan, S. L. W., & Recchi, S. 2008, *MNRAS*, 391, 825
- Decressin, T., Baumgardt, H., Charbonnel, C., & Kroupa, P. 2010, *A&A*, 516, A73
- Da Costa, G. S., Held, E. V., Saviane, I. & Gullieuszik, M. 2009, *ApJ*, 705, 1481
- di Criscienzo, M. et al., 2011, *MNRAS*, 414, 3381
- Dixon, W. V. D., Davidsen, A. F., Dorman, B., & Ferguson, H. C. 1996, *AJ*, 111, 1936
- Fitch, W. S. & Szeidl, B. 1976, *ApJ*, 203, 616
- Ferraro, F. R., Clementini, G., Fusi Pecci, F., Sortino, R., & Buonanno, R. 1992, *MNRAS*, 256, 391
- Ferraro, F.R., Dalessandro, E., Mucciarelli, A. et al. 2009, *Nature*, 462, 483
- Freeman, K. C. & Rodgers, A. W. 1975, *ApJ*, 201, L71
- Gratton, R. G., Lucatello, S., Carretta, E., Bragaglia, A., D’Orazi, V. & Momany, Y. 2011, *A&A*, 534, 123
- Gratton, R.G. et al. 2012a, *A&A*, 539, 19
- Gratton, R.G., Lucatello, S., Sollima, A., et al. 2013, *A&A*, 549, 41
- Grundahl, F., VandenBerg, D. A., & Andersen, M. I. 1998, *ApJ*, 500, L179
- Grundahl, F., Catelan, M., Landsman, W.B., Stetson, P.B., & Andersen, M.I. 1999, *ApJ*, 524, 242
- Guldenschuh, K. A. et al. 2005, *PASP*, 117, 721
- Johnson, C.I. & Pilachowski, C.A. 2012, 754, 38
- Harris, W. E. 1996, *AJ*, 112, 1487
- Harris W. E., Racine R., 1979, *ARA&A*, 17, 241
- Hesser J. E., 1976, *PASP*, 88, 849
- Hesser, J. E., Hartwick, F. D. A., & McClure, R. D. 1977, *ApJS*, 33, 471
- Hesser, J. E., & Harris, G. L. H. 1979, *ApJ*, 234, 513
- Hesser, J. E. & Hartwick, F.D.A. 1979 *ApJ* 234, 513
- Hoffleit, D. 1972, *IBVS*, 660
- Iannicola, G., Monelli, M., Bono, G. et al. 2009, *ApJ*, 696, 120
- Jurcsik, J., et al. 2009, *MNRAS*, 400, 1006
- Kraft, R. P. & Ivans, I. I. 2003, *PASP*, 115, 143
- Kaluzny, J. & Thompson, I. B. 2001, *A&A*, 373, 899
- Kinman, T.D. & Brown, W.R. 2010, *AJ*, 139, 2014
- Klepikova, L. A. 1956, *Perem. Zvezdy (Var. Stars)*, 11, 1
- Kravtsov, V V., Samus, N. N., Alcaïno, G. & Liller, W. 1994, *Ast. Letters*, 20, 339
- Kolenberg, K. 2011, *Carnegie Observatories Astroph. Ser.*, 5, 100
- Kuehn, C.A., Smith, H.A., Catelan, M., Pritzl, B.J., De Lee, N. & Borissova, J. 2011, *AJ*, 142, 107
- Kunder, A., Popowski, P., Cook, K. H., Nikolaev, S., & Chaboyer, B. 2008, *AJ*, 135, 631
- Kunder, A.M., Chaboyer, B. 2009, & Layden, A. 2010 *AJ*, 139, 415
- Kunder, A.M., Walker, A.R., Stetson, P.B. et al. 2011, *AJ*, 141, 15
- Kunder, A., Salaris, M., Cassisi, S., de Propris, R., Walker, A., Stetson, P.B., Catelan, M. & Amigo, P. 2013, *AJ*, 145, 25
- Kunder, A., Stetson, P.B., Catelan, M., Walker, A. & Amigo, P., 2013, *AJ*, 145, 33
- Lardo, C., Bellazzini, M., Pancino, E., Carretta, E., Bragaglia, A. & Dalessandro, E. 2011, *A&A*, 525, 114
- Landolt, A.U. 1973, *AJ*, 78, 959
- Landolt, A.U. 1983, *AJ*, 88, 439
- Landolt, A.U. 1992, *AJ*, 104, 340
- Layden, A.C. 1998, *AJ*, 115, 193;
- Layden, A.C. & Sarajedini, A. 2000, *AJ*, 119, 1760
- Layden, A. & Sarajedini, A. 2003, *AJ*, 125, 208
- Le Borgne, L. F., Vandenbroere, J., Poretti, E., Klotz, A., Boër, D. Y., Martignoni, M., & Acerbi, F. 2007, *A&A*, 476, 307
- Le Borgne, J.-F., Klotz, A., Poretti, E. *AJ*, 144, 39
- Lee, Y.-W., Demarque, P., & Zinn, R. 1994, *ApJ*, 423, 248
- Lee, Y.-W., Gim, H.B., & Casetti-Dinescu, D.I. 2007, *ApJ*, 661, 49L
- Lee, J.-W., Kang, Y.-W., Lee, J., & Lee, Y.-W. 2009, *Nature*, 462, 480
- Joo, S.-J. & Lee, Y.-W. 2013, *ApJ*, 762, 36
- Lloyd Evans, T. 1978, *MNRAS*, 182, 293
- Mackey, A. D., & van den Bergh, S. 2005, *MNRAS*, 360, 631
- Mateo, M., Udalski, A., Szymanski, M., Kaluzny, J., Kubiak, M., & Krzemiński, W. 1995, *AJ*, 109, 588
- Marconi, M. 2009, *AIPC*, 1170, 223
- Marconi, M., Bono, G., Caputo, F., Piersimoni, A.M., Pietrinferni, A., Stellingwerf, R. F. 2011, *ApJ*, 738, 111
- Marino A. F., Villanova S., Piotto G., Milone A. P., Momany Y., Bedin L. R., Medling A. M., 2008, *A&A*, 490, 625
- Marino, A. F., Milone, A. P., Piotto, G., Villanova, S., Bedin, L. R., Bellini, A. & Renzini, A. 2009, *A&A*, 505, 1099
- Marino, A. F., Sneden, C., Kraft, R. P., et al. 2011a, *A&A*, 532, 8
- Marino, A. F., Villanova, S., Milone, A. P., Piotto, G.; Lind, K., Geisler, D. & Stetson, P. B., 2011b, *ApJ*, 730, 16
- Marino, A. F., Milone, A. P., Sneden, C. et al. 2012a, *A&A*, 541, 15

- Marino, A. F., Milone, A. P., Piotto, G., et al. 2012b, *ApJ*, 746, 14
- Marino, A. F., Milone, A. P. & Lind, L. 2013, accepted in *ApJ*, arXiv:1302.5870
- McCall, M.L. 2004, *AJ*, 128, 2144
- Milone, A. P., Stetson, P. B., Piotto, G., Bedin, L. R., Anderson, J., Cassisi, S. & Salaris, M. 2009, *A&A*, 503, 755
- Milone, A. P., Piotto, G., Bedin, L. R., Marino, A. F., Momany, Y. & Villanova, S. 2012a, *MSAIS*, 19, 173
- Milone, A. P., Piotto, G., Bedin, L. R. et al. 2012b, *ApJ*, 744, 58
- Mironov, A. V. 1972, *AZh*, 49, 134
- Moehler, S., Dreizler, S., Lanz, T. et al. 2011, *A&A*, 526, A136
- Monaco, L., Pancino, E., Ferraro, F.R. & Bellazzini, M. 2004, *MNRAS*, 349, 1278
- Monelli, M., Milone, A.P., Stetson, P.B. et al. 2013, arXiv:1303.5187
- Moskalik, P. Poretti, E. 2003, *A&A*, 398, 213
- Mucciarelli, A., Bellazzini, M., Ibatá, R., Merle, T., Chapman, S. C., Dalessandro, E. & Sollima, A. 2012, *MNRAS*, 426, 2889
- Norris J. E., 2004, *ApJ*, 612, L25
- Norris, J., & Freeman, K. C. 1983, *ApJ*, 266, 130
- Norris, J. E. & Da Costa, G. S. 1995, *ApJ*, 447, 680
- Pancino, E., Pasquini, L., Hill, V., Ferraro, F. R., & Bellazzini, M. 2002, *ApJ*, 568, L101
- Peniche, R., Pena, J.H., Gomez, T. & Parrao, L. 1989, *A&A*, 209, 59
- Pietrinferni, A., Cassisi, S., Salaris, M., & Castelli, F. 2004, *ApJ*, 612, 168
- Pietrinferni, A., Cassisi, S., Salaris, M., & Castelli, F. 2006, *ApJ*, 642, 797
- Pietrinferni, A., Cassisi, S., Salaris, M., Percival, S. & Ferguson, J.W. 2009, *ApJ*, 697, 275
- Pietrukowicz, P. & Kaluzny, J. 2003, *AcA*, 53, 371
- Pietrukowicz, P., Kaluzny, J., Thompson, I. B., Jaroszynski, M., Schwarzenberg-Czerny, A., Krzeminski, W., Pych, W., 2005, *Ac. Ast.*, 55, 261
- Pietrukowicz, P., Udalski, A., Soszyński, I. et al. 2012, *ApJ*, 750, 169
- Piotto, G., Zoccali, M., King, I.R., Djorgovski, S.G., Sosin, C., Rich, R.M. & Meylan, G. 1999, *AJ*, 118, 1727
- Piotto G. et al., 2005, *ApJ*, 621, 777
- Piotto G. et al., 2007, *ApJ*, 661, L53
- Piotto, G., Milone, A. P., Anderson, J., et al. 2012, *ApJ*, 760, 39
- Pritzl, B. J., Smith, H. A., Catelan, M., & Sweigart, A. V. 2000, *ApJ*, 530, 41
- Pritzl, B. J., Smith, H. A., Catelan, M., & Sweigart, A. V. 2001, *AJ*, 122, 2600
- Pojmański, G. *Acta Astronomica* 50, 177, 2000
- Richter, P.; Hilker, M.; Richtler, T. 1999, *A&A*, 350, 476
- Ripepi, V., Clementini, G., Di Criscienzo, M. et al. 2007, *ApJ*, 667, 61
- Robin, A.C., Reylé, C., Derrière, S. & Picaud, S. 2003, *A&A*, 409, 523
- Rood, R. T., & Crocker, D. A. 1989, in *IAU Colloq.* 111, *The Use of Pulsating Stars in Fundamental Problems of Astronomy*, ed. E. G. Schmidt (Cambridge: Cambridge Univ. Press), 103
- Salaris, M., Cassisi, S., & Pietrinferni, A. 2008, *ApJL*, 678, L25
- Sandage, A. 1990, *ApJ*, 350, 603
- Saviane, I., da Costa, G. S., Held, E. V., Sommariva, V., Gullieuszik, M., Barbuy, B. & Ortolani, S. 2012, *A&A*, 540, 27
- Sawyer, H. B. 1944, *DDO Publ.*, 1, No. 15
- Sbordone, L., Salaris, M., Weiss, A. & Cassisi, S. 2011, *A&A*, 534, 9
- Schlafly, E.F. & Finkbeiner, D.P. 2011, *ApJ*, 737, 103
- Schlegel, D.J., Finkbeiner, D.P. & Davis, M. 1998, *ApJ*, 500, 525
- Schultz, G. V., & Wiemer, W. 1975, *A&A*, 43, 133
- Shapley, H. 1927, *Harv. Bull.*, 848
- Sdor, A., Jurcsik, J., Molnár, L. et al. 2012, *ASPC*, 462, 228
- Sollima, A., Borissova, J., Catelan, M., Smith, H. A., Minniti, D., Cacciari, C. & Ferraro, F. R. 2006, *ApJL*, 640, 43
- Sollima, A., Ferraro, F. R., Bellazzini, M., et al. 2007, *ApJ*, 654, 915
- Sollima, A., Cacciari, C., Bellazzini, M. & Colucci, S. 2010, *MNRAS*, 406, 329
- Stetson, P.B. 1987, *PASP*, 99, 191
- Stetson, P.B. 1990, *PASP*, 102, 932
- Stetson, P.B. 1994, *PASP*, 106, 250
- Stetson, P.B. 2000, *PASP*, 112, 925
- Stetson, P.B., Bruntt, H. & Grundahl, F. 2003, *PASP*, 115, 41
- Stetson, P.B., Catelan, M. & Smith, H.A. 2005, *PASP*, 117, 1325
- Sturch, C. 1966, *ApJ*, 143, 774
- Szabo et al. *MNRAS*, 409, 1244, 2010
- van Albada, T.S., & Baker, N. 1973, *ApJ*, 185, 477
- Walker, A.R. 1990, *AJ*, 100, 1532
- Walker, A.R. 1994, *AJ*, 108, 555
- Walker, A.R. 1998, *AJ*, 116, 220
- Walker, A.R., Kunder, A.M. & Andreuzzi, G. 2011, *MNRAS*, 415, 643
- Wehlau, A. & Sawyer Hogg, H. 1977, *AJ*, 82, 137
- Wehlau, A. & Sawyer Hogg, H. 1978, *AJ*, 83, 946
- Zinn, T. & West, M.J. 1984, *ApJS* 55,45
- Zloczewski, K., Kaluzny, J., Rozyczka, M., Krzeminski, W., Mazur, B. & Thompson, I. B. 2013, arXiv1301.1198
- Zoccali, M., Pancino, E., Catelan, M., et al. 2009, *ApJ*, 697, L22
- Zorotovic, M. et al. 2010, *AJ*, 139, 357